ANNUAL TECHNICAL REPORT

Contract AF 19(628)-5100
1 September 1968

Department of Geophysics and Geophysical Engineering

Saint Louis University

ARPA Order Number: 292, Amendment 45
Project Code Number: 5810
Contractor: Saint Louis University
Date of Contract: 1 September 1965
Contract Number: AF 19(628)-5100
Amount of Contract: $530,985
Contract Expiration Date: 31 August 1969
Project Director: Carl Kisslinger, JE 5-3300/540
Title of Work: Research in Seismology

Table of Contents

Annual Technical Report

Introduction

In this report, research in seismology on fundamental problems related to the detection, location, and identification of underground nuclear explosions is described. The period covered by the report is September, 1967 through August, 1968.

The personnel engaged in this work are all associated with the Department of Geophysics and Geophysical Engineering, Institute of Technology, Saint Louis University. Scientists in charge of work on various tasks under the project are: S. J. Duda, C. Kisslinger, O. W. Nuttli, and W. V. Stauder. In addition, ten research assistants, all graduate students in geophysics, contributed to the research.

In the report, the completion of a study of Love and Rayleigh wave propagation in the central part of North America is described. Observational and theoretical studies of seismic body waves, P and S, follow, and finally, research in model seismology is described.

A. Work in Progress.

1. Long Period P-Wave Amplitudes at LASA.

The object of this study is to investigate the amplitude anomalies of the long period P waves at LASA as a function of distance and azimuth to the source region, with emphasis upon the interpretation of the anomalies in terms of crust and upper mantle structure.

Two approaches to this problem have been taken. One compares P amplitudes at the individual stations for a given earthquake, to determine: 1) if any particular station has consistently larger or smaller amplitudes relative to the other stations; 2) if there is an amplitude variation across the array which is a function of distance and azimuth; and 3) if there are any epicentral distances for which the change of amplitude with distance is abnormally large, indicative of rapid velocity change with depth in the mantle. The second approach uses the departure of the P motion from the great circle path as determined from the amplitudes of the horizontal components of ground motion at the individual stations of the array. These departures from the great circle path, or azimuth anomalies, are theoretically related in a relatively straightforward manner to the lateral changes in velocity that may exist beneath LASA.

Much effort was devoted to the latter approach, particularly in the gathering of data, because the method has the potential of yielding in a direct manner information about the dip or horizontal velocity changes of the subsurface layers. The data, however, exhibited an amount of scatter equal at least in size to any existing anomaly, and attempts to reduce the scatter proved fruitless. For this reason that part of the study has been dropped. However, because no similar studies have been reported in the literature, some discussion of the difficulties encountered is included here.

The basic data were copies of the Develecorder films of the long period seismograms of the D and F rings. Earthquakes which produced impulsive P waves at LASA, were selected with the

additional requirements that the microseismic background level was low and that the P amplitudes were large but not so large as to have the turning points of the motion fall off the film. In the first attempt to obtain the necessary data the amplitudes of the zero-to-first maximum (or minimum) and the first maximum-to-first minimum were read with the assistance of a film digitizer. These horizontal amplitude components were combined to give an observed direction of wave arrival (O) and compared with the computed azimuth (C) of the great circle path at the station. Results for some of the earthquakes studied are given in Table 1.

Table 1

Earthquake Date	Origin Time	Lat.	Long.	Station	O_1*	O_2**	C	O_1-C	O_2-C
13 May 67	05-18-55.4	56.5N	152.6W	D-1	314.1°	309.3°	306.1°	+8.0°	+3.2°
				D-2	315.0	308.8	306.6	+8.4	+2.2
				D-3	311.2	301.4	306.5	+4.7	-5.1
				F-3	--	309.6	307.3	--	+2.3
				F-4	--	310.5	305.3	--	+5.2
21 May 67	07-18-12.8	27.9N	111.3W	D-1	195.3	194.8	194.6	+0.7	+0.2
				D-2	202.4	201.4	194.5	+7.9	+6.9
				D-3	194.9	187.9	193.2	+1.7	-5.3
				D-4	195.8	--	193.2	+2.6	--
				F-1	197.3	199.2	196.0	+1.3	+3.2
				F-2	191.4	203.5	196.4	-5.0	+7.1
				F-3	193.2	191.0	191.9	+1.3	-0.9
				F-4	194.2	192.2	191.5	+2.7	+0.7
01 Jul 67	23-10-07.2	54.4N	158.0W	D-1	296.1	--	302.7	-6.6	--
				D-2	298.4	--	303.1	-4.7	--
				D-3	292.4	--	302.9	-10.5	--
				D-4	296.2	--	302.4	- 6.2	--
				F-4	297.2	--	301.7	-4.5	--
29 Jul 67	10-24-24.6	6.8N	73.0W	D-1	137.1	--	134.3	+2.8	--
				D-2	133.3	--	133.9	-0.6	--
				F-3	130.3	--	132.3	-2.0	--
				F-4	137.3	--	133.4	+3.9	--

* From first half-amplitude

** From first peak to peak motion

No pattern of regularity appeared in the O-C data of Table 1 and in other similar data not included in this report. In fact, when these O-C data were plotted against the azimuth of the great circle path it was found for each of the azimuths for which there were sufficient data (130°, 190°, and 310°) that the negative and positive values of the O-C were about equal in value and in number. This indicates that the cause of the anomalies is some type of reading or instrumental effect rather than lateral velocity variations in the crust and mantle.

Although the earthquakes selected for study had relatively small microseismic and instrumental noise amplitudes, it is possible that a peak in noise motion could arrive simultaneously and interfere with a peak in the P wave motion. Azimuths calculated from peak amplitudes of the P motion would thus be in error. This difficulty can be obviated, however, by the use of particle motion diagrams if the amplitude of the noise is small compared to that of the signal and if both do not have the same frequency content.

Figure 1 contains horizontal component particle motion diagrams for the P waves of 21 May 1967 as recorded at the D-1 and F-4 stations. It can be seen from this figure that the motion is approximately, but not exactly, linear. As a result of this departure from linearity there is uncertainty in the value assigned to the direction of the particle motion. Table 2 contains the direction of a visual estimate of a straight line fit to the motion in the first and third quadrants, and the corresponding departure from the great circle path for all the stations of the D and F rings for the earthquake of 21 May 1967.

Sample Particle Motion Diagrams of P
Earthquake of May 21, 1967

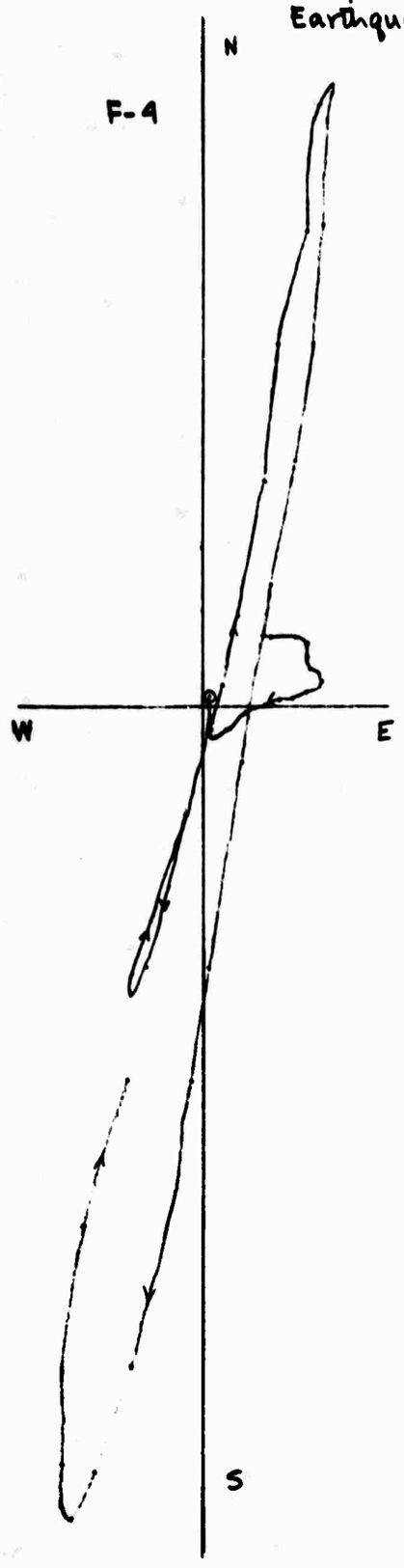

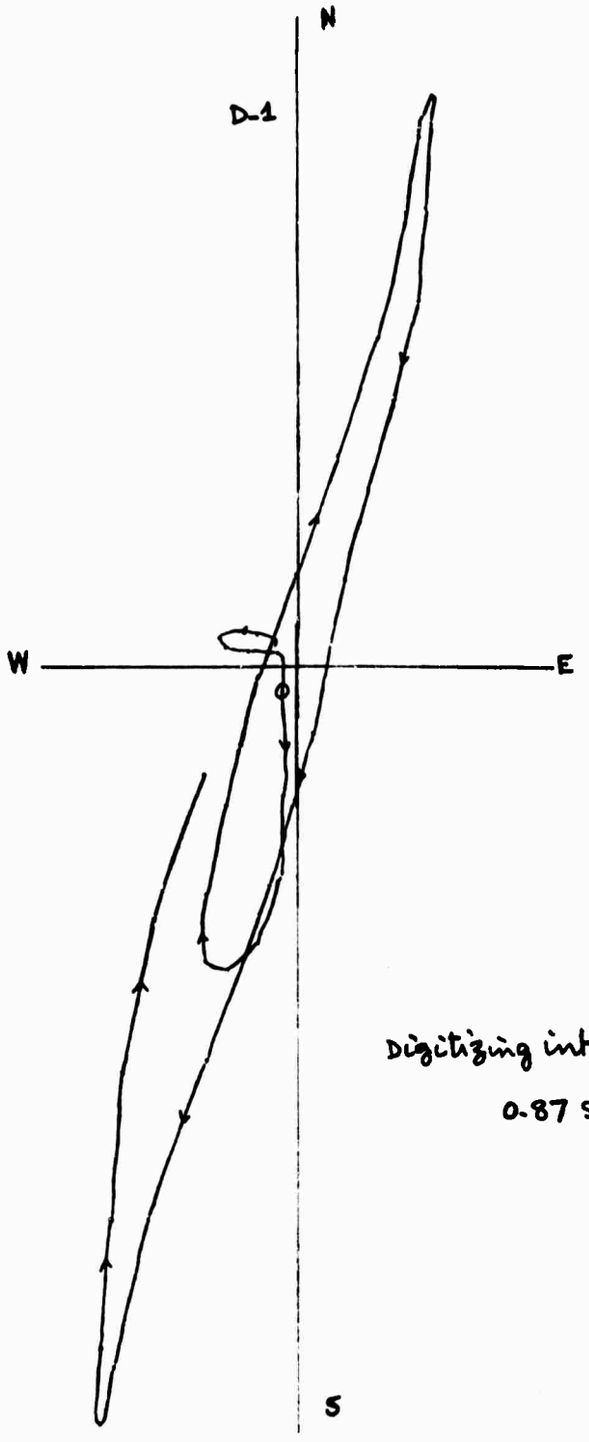

Digitizing interval
0.87 Seconds

Figure 1

Table 2

Station	O_I*	O_I-C	O_{III}**	O_{III}-C
D-1	197.4°	+2.8°	196.9°	+2.3°
D-2	198.4	+3.9	200.9	+6.4
D-3	191.9	-1.3	193.1	-0.1
D-4	190.5	-2.7	188.4	-4.8
F-1	190.8	-5.2	194.4	-1.6
F-2	204.5	+8.1	202.1	+5.7
F-3	187.4	-4.5	193.2	+1.3
F-4	188.5	-3.0	193.8	+2.3

* From motion in first quadrant.
** From motion in third quadrant.

Finally, to remove the subjectivity involved in assigning a direction to the particle motion "by eye," a least-squares fit of a straight line was made to the data. The results are summarized in Table 3.

Table 3

Station	O_1*	O_1-C	O_2**	O_2-C
D-1	189.4°	-5.2°	195.6°	+1.0°
D-2	197.9	+3.4	196.5	+2.0
D-3	196.7	+3.5	193.4	+0.2
D-4	191.1	-2.1	187.9	-5.3
F-1	198.7	+2.7	192.4	-3.6
F-2	194.9	-1.5	203.6	+7.2
F-3	198.2	+6.3	189.2	-2.7
F-4	196.8	+5.3	190.8	-0.7

*From first half-amplitude.
**From first peak to peak motion.

The values contained in Tables 1 and 3 should be similar, although comparison indicates no such agreement, even insofar as the sign of the O-C's is concerned. Because the values given in Table 2 were determined from several cycles of the P motion, they are expected to be somewhat different than those in Tables 1 and 3. In any case, if dip of the M discontinuity or lateral velocity variations in the mantle under LASA were responsible for the

azimuth anomalies, then for a given earthquake all the O-C's should have the same sign and have about the same value at all the LASA stations. It can be seen from the tables that positive and negative values of O-C for the earthquake of 21 May 1967 are about equal in number.

It is concluded that the observed azimuth anomalies are most probably caused by some combination of microseisms, instrumental noise, local and very shallow station site irregularities, and possibly small errors in instrument calibration and seismometer orientation. Their combined effects appear to produce an apparent azimuth anomaly of as much as 5° in absolute value.

The second approach to amplitude anomaly studies of long period P at LASA has proved more fruitful, even though the work is in a preliminary state. One important conclusion is that the long period P wave closely maintains its waveform and amplitude across LASA, with departures of individual station amplitudes from the mean amplitude usually no greater than ten percent. This suggests that long period P waves are ideally suited for such processing techniques as delay and sum, etc., whenever the seismic source is of sufficiently large magnitude to generate them.

Table 4 contains the hypocentral coordinates of nine earthquakes used in this part of the study. The epicentral distance, azimuth, and vertical component P wave amplitude, as well as the departure from the average amplitude of an individual station's amplitude, are given for the nine earthquakes in Table 5. The amplitudes given in Table 5 are peak to peak values, measured from the first maximum to the first minimum, or vice versa.

Table 4

Earthquake Number	Date	Origin Time	Lat.	Long.	Depth	Magnitude
1	21 May 67	07-18-12.8	27.9N	111.3W	33 km	4.7
2	18 Oct 67	01-11-44.8	79.8N	2.4E	33	5.7
3	13 May 67	05-18-55.4	56.5N	152.6W	33	5.3
4	27 May 67	17-22-58.7	51.9N	176.1E	34	5.8
5	16 May 67	12-58-09.5	13.5N	90.6W	95	4.8
6	19 Jun 67	17-07-45.4	52.7N	166.9W	33	5.7
7	10 Dec 67	12-06-50.3	40.5N	124.6W	5	5.8
8	20 May 68	20-05-49.06	30.7S	178.4W	46	6.0
9	21 May 68	08-20-00.86	44.9N	150.1E	normal	5.7

Table 5

Station	Earthquake Number	Distance	Azimuth	Z amplitude (milimicrons)	% departure from mean
D-1	1	19.4°	194.6°	37.5	-10.7
	2	47.4	13.3	91.8	- 7.3
	3	30.0	306.1	13.2	-20.9
	4	48.8	306.3	49.9	- 6.9
	5	35.6	153.9	15.1	+12.7
	6	38.8	301.8	23.1	-11.1
	7	14.9	251.7	107.5	-14.5
	8	101.0	236.8	172.8 (?)	-29.6 (?)
	9	66.8	311.3	35.1	- 1.9
D-2	1	19.0	194.5	39.3	- 6.4
	2	47.7	13.2	94.3	- 4.7
	3	30.1	306.6	14.6	-12.6
	4	48.9	306.5	51.4	- 4.1
	5	35.4	153.5	12.2	- 8.9
	6	38.9	302.1	23.6	- 9.2
	7	14.7	252.7	--	--
	8	100.8	236.7	271.8	+10.7
	9	66.9	311.4	35.6	- 0.5
D-3	1	19.0	193.2	42.1	+ 0.2
	2	47.8	13.2	105.9	+ 1.5
	3	29.8	306.5	18.0	+ 7.8
	4	48.6	306.3	57.0	+ 6.3
	5	35.6	152.7	10.2	-23.9 (?)
	6	38.6	302.0	28.3	+ 8.8
	7	14.4	251.8	117.4	- 6.6
	8	100.5	236.4	--	--
	9	66.7	311.1	--	--
D-4	1	19.4	193.2	44.2	+ 5.2
	2	47.4	13.3	99.5	+ 0.5
	3	29.6	306.0	19.6	+17.4
	4	48.4	306.0	57.8	+ 7.8
	5	35.9	153.1	13.7	+ 2.2
	6	38.4	301.6	27.1	+ 4.2
	7	14.6	250.5	116.4	- 7.4
	8	100.8	236.5	241.7	- 1.5
	9	66.5	311.0	35.8	0.0

Station	Earthquake Number	Distance	Azimuth	Z amplitude (milimicrons)	% departure from mean
F-1	1	20.0	196.0	42.4	+ 0.9
	2	46.7	13.5	--	--
	3	30.1	305.4	14.6	-12.6
	4	48.8	306.2	59.9	+11.7
	5	35.9	155.3	14.6	+ 8.9
	6	38.9	301.4	31.9	+22.7
	7	15.5	250.9	168.1 (?)	+33.7 (?)
	8	101.7	237.4	255.5	+ 4.1
	9	66.8	311.5	39.5	+10.3
F-2	1	18.5	196.4	39.8	- 5.2
	2	48.2	13.1	92.7	- 6.4
	3	30.8	307.4	15.8	- 5.4
	4	49.5	307.1	48.7	- 9.1
	5	34.7	153.9	13.5	+ 0.7
	6	39.5	302.9	19.1	-26.5
	7	14.9	255.6	134.5	+ 7.0
	8	100.8	236.9	229.1	- 6.6
	9	67.6	311.8	29.5	-17.6
F-3	1	18.3	191.9	44.3	+ 5.4
	2	48.4	13.0	98.8	- 0.2
	3	29.8	307.3	18.0	+ 7.8
	4	48.6	306.5	52.9	- 1.3
	5	35.2	151.4	13.9	+ 3.7
	6	38.5	302.4	23.8	- 8.5
	7	13.9	253.0	130.6	+ 3.9
	8	99.9	235.9	252.6	+ 2.9
	9	66.7	311.0	34.8	- 2.8
F-4	1	19.8	191.5	46.3	+10.2
	2	47.0	13.3	106.4	+ 7.5
	3	29.1	305.3	20.2	+20.9
	4	47.8	305.5	51.4	- 4.1
	5	36.5	152.6	13.7	+ 2.2
	6	37.9	300.9	31.9	+22.7
	7	14.4	247.9	105.8	-15.8
	8	100.8	236.2	295.1 (?)	+20.2 (?)
	9	65.9	310.6	40.4	+12.8

From Table 5 it can be observed that stations D-1, D-2, and F-2 exhibit a tendency to have amplitudes less than the average, whereas D-3, D-4, F-1, and F-4 have amplitudes greater than the average. These observations, however, are based upon a small amount of data and may be changed as more data accumulate.

There are at present insufficient data to determine if the amplitudes have any azimuthal dependence. For the epicentral distance intervals studied there is no indication of a rapid decrease

or increase in amplitude with increasing epicentral distance, such as are produced by discontinuous increases in the velocity gradient in the mantle. However, as yet data is lacking for some epicentral distances.

To repeat, the most important conclusion to be drawn from the amplitude observations to date is the coherence of the long period P waveform across LASA, with the amplitude of P at an individual station usually differing by no more than ten percent from the average of the values at all the stations of the D and F rings.

2. Body Wave Travel Time Anomalies

Statement of the Problem.

Travel-time tables of body waves (e.g. Jeffreys-Bullen) bear information concerning the average structure of the Earth. Travel time anomalies, observed at various places over the Earth, indicate heterogeneities in the Earth's structure. The problem investigated is 1) to measure the travel times and find statistically significant deviations from the mean, 2) to determine the probable location of the anomalous structure, and 3) to interpret the anomalies from a tectonophysical point of view.

In return, it is expected that the more detailed knowledge of the travel-time anomalies and the structure of the Earth will increase the accuracy of epicenter determination of natural and artificial events on the Earth.

In continuation of previous efforts (see Annual Technical Report Contract AF 19(628)-5100, September 1967, (ATR 1967), P Time Delays and Continental Uplift) the investigation has been extended in the following directions:

1. determination of the first derivatives of the travel-time curve from observations of P-arrivals in the area previously found to have anomalous relative P-time delays (RPF);
2. finding of a theoretical model of crust and upper mantle yielding relative P-time delays and first derivatives of the travel-time curve consistent with the observed ones;
3. application of the previous approaches with some modifications to S-wave travel times.

Determination of first derivatives of P-wave travel times.

From the arrival times of P-waves at two stations and the epicentral distances of the earthquake, the derivative of the travel-time curve can be computed. If regional anomalies are being studied, the stations must not only have similar epicentral distances, but also be situated close to each other. The derivative then characterizes the structure between the two stations. In Fennoscandia, the region selected for the research for reasons outlined in ATR 1967, inhomogeneities in the structure seem to exist over relatively short distances. If the distance between the two stations is too large, the anomaly in the derivative, if existent, would lose its meaning. Therefore, the derivatives were not computed for all possible combinations of 15 stations into pairs, but were computed for all station pairs for which the distance between the stations did not exceed about 300 mi. The derivatives were classified according to the azimuths toward epicenters into four groups (N, E, S, W), and displayed as functions of epicentral distance. Due to the natural distribution of seismically active regions, most earthquakes arrived from

northerly and easterly directions, and the derivatives in those groups (N, E) are of primary interest. The derivatives in the other two groups (S, W) are not used as independent evidence, but only as supporting the conclusions. From a detailed analysis of all the derivatives it was found that for some station pairs the derivative deviates significantly either in the positive or negative direction, while for some station pairs no deviation is found. Fig. 2 gives samples of all three cases.

No deviation of the derivative from the expected value means that there is no lateral change in the structure between the station pair, but an anomalous structure, uniform over the distance between the stations, cannot be excluded. A positive or negative deviation of the derivative means a lateral change in the structure between the stations. Here it is implied that the source of the anomaly in the derivative of the travel-time curve, as for the RPD's (see ATR 1967), lies in the uppermost part of the earth, beneath the station. This assumption seems justified for at least two reasons:

i.) Measurable lateral inhomogeneities in the Earth are more probable at shallower depths than at greater depths because of the increasing role of hydrostatic pressure at greater depths, tending to create spherically symmetric conditions around the center of the Earth, and because of tectonic forces and tectonic structures known with some certainty to be inhomogeneous down at least to the Moho-discontinuity, and probably deeper.

ii.) The two seismic rays originating at the earthquake focus and terminating at the station pair under consideration

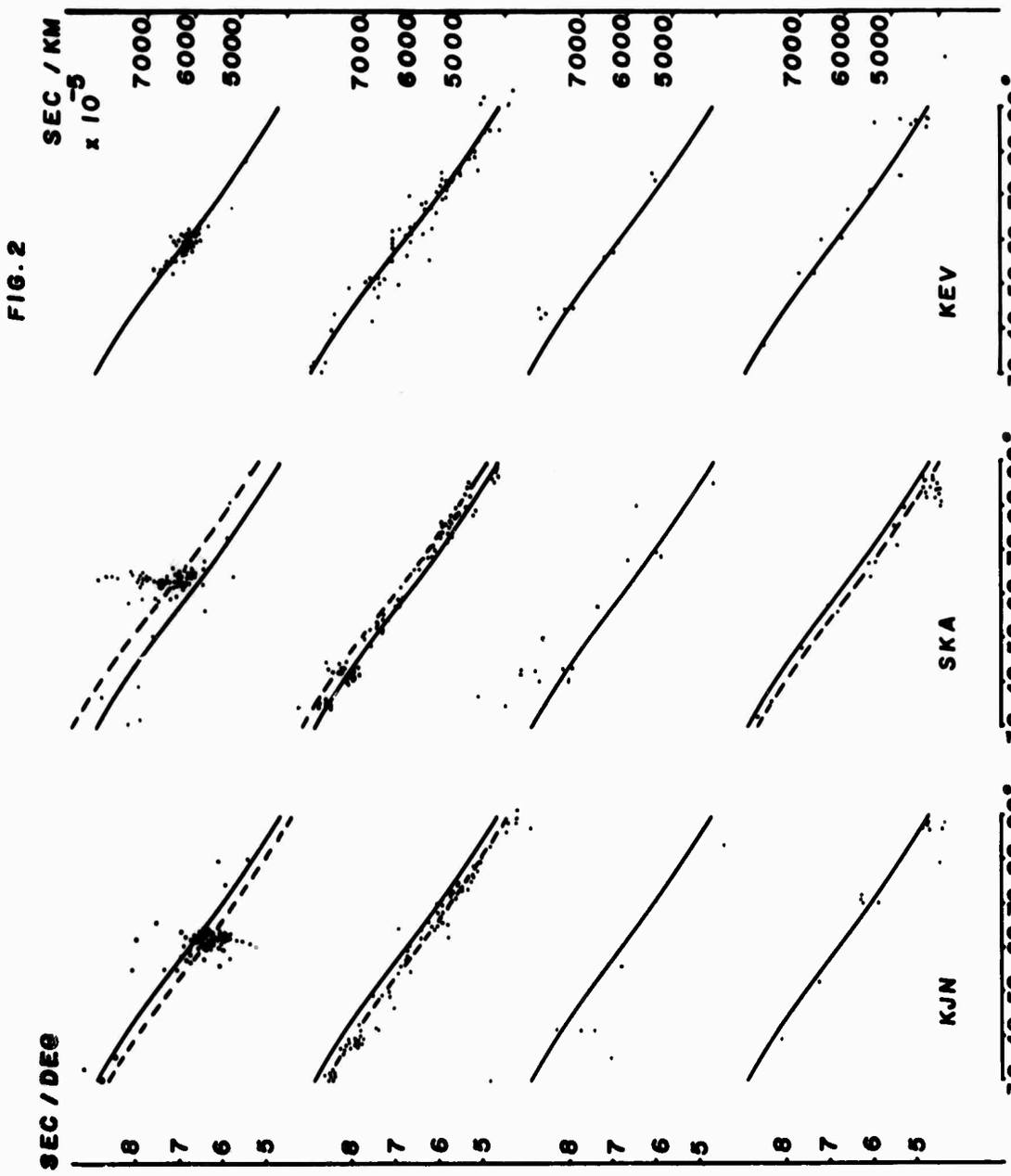
SEC / KM
x 10^-5
7000
6000
5000
KEV
SKA
KJN
30 40 50 60 70 80 90°
SEC / DEG
8 7 6 5

FIG. 2

FIG. 2

diverge from each other mainly just prior to the arrival at the stations. Thus, beneath the stations they are most likely to traverse anomalous structures and suffer a relative acceleration or deceleration.

This assumption is supported by the evidence of Fig. 2. SKA, UME, and KJN are three of the studied stations, situated on a roughly E-W striking line crossing Fennoscandia. The epicenters in group N lie mainly in the Aleutian Islands, north-northeast of Fennoscandia. The derivatives between SKA-UME and KJN-UME were computed. The arrival times produce a distinct positive anomaly at SKA-UME and a distinct negative one at KJN-UME. Similarly, the epicenters in group E produce a slightly positive anomaly at SKA-UME and a clear negative one at KJN-UME. It is also interesting to note that in SKA-UME, while the anomaly for earthquakes from easterly directions (group E) are positive, as mentioned, the anomaly for earthquakes from westerly directions (group W) are negative, as far as can be seen from the limited number of epicenters in the last group. These features will be explained below with the help of a postulated model.

Theoretical model of crust and upper mantle.

The derivatives of the travel-time curve for various epicentral distances were computed and analyzed for a total of 20 station pairs. The findings are concordant with those of an analysis of the relative P-time delays insofar as higher velocities in the central portion of Fennoscandia are indicated. In addition, the derivatives, because of closer spacing of the observation points, permit the delineation of the limits of regions of anomalous velocities. A corresponding contour map is under construction.

As the basis of the analysis a layer of constant thickness with seismic velocity increasing both with depth and horizontally is considered. A vertical cross-section parallel to the horizontal velocity gradient is shown in Fig. 3. Two stations are thus situated at points with different velocities. The vertical velocity increase is the same over the entire layer and will not cause any RPD's different from zero or anomalies in the derivatives of the travel-time curves. The velocity in the vertical direction is then assumed constant and equal to an average value. The velocity change in the horizontal direction is responsible for the RPD's different from zero and for anomalous derivatives. The effect of a linear horizontal velocity increase upon the derivatives was computed for different spacings, DX, between and positions, XI, of the stations, for different thicknesses H and different rates of increase "a" of the velocity in the horizontal direction. A sample computation is presented in Fig. 4, in which the anomalies of the first derivative of the P-travel-time curve as a function of epicentral distance under varying specified conditions are shown. A comparison of the observed and computed anomalies indicates that the thickness of the layer with a horizontal velocity inhomogeneity is relatively thin, of the order of 50 km. Under this circumstance RPD's result with maximum values and variations with azimuth are in agreement with earlier observations. Accordingly, it is considered most likely that a horizontal velocity gradient exists beneath Scandinavia.

Consideration of possible causes of the anomaly has led to the conclusion that it may be related to the geologically recent

FIG. 3

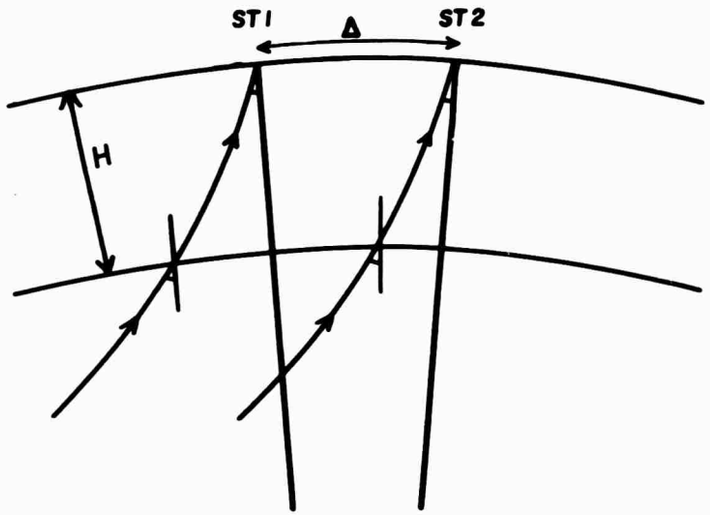

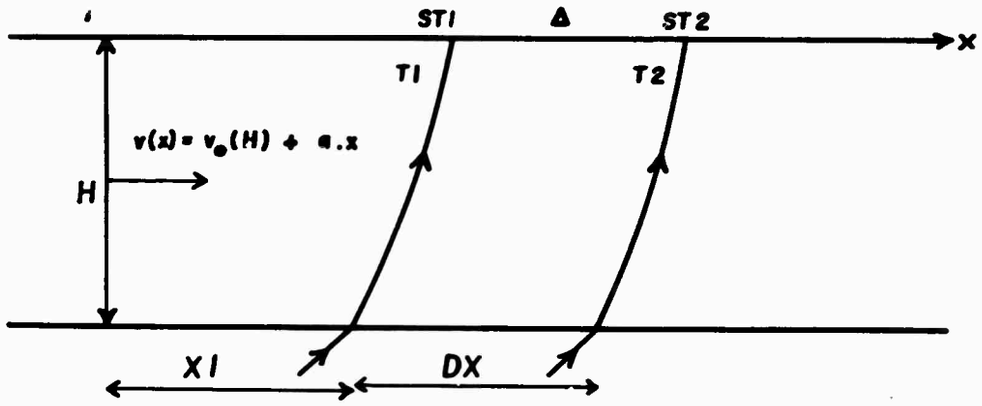

horizontal velocity gradient in layer H :

1 : zero $\Longrightarrow$

2 : non −zero $\Longrightarrow$

slope of travel time curve $\begin{cases} \dfrac{T2 - T1}{\Delta} = A \\ \dfrac{(T2 - \delta T2) - (T1 - \delta T1)}{\Delta} = A + \delta A \end{cases}$

FIG. 4

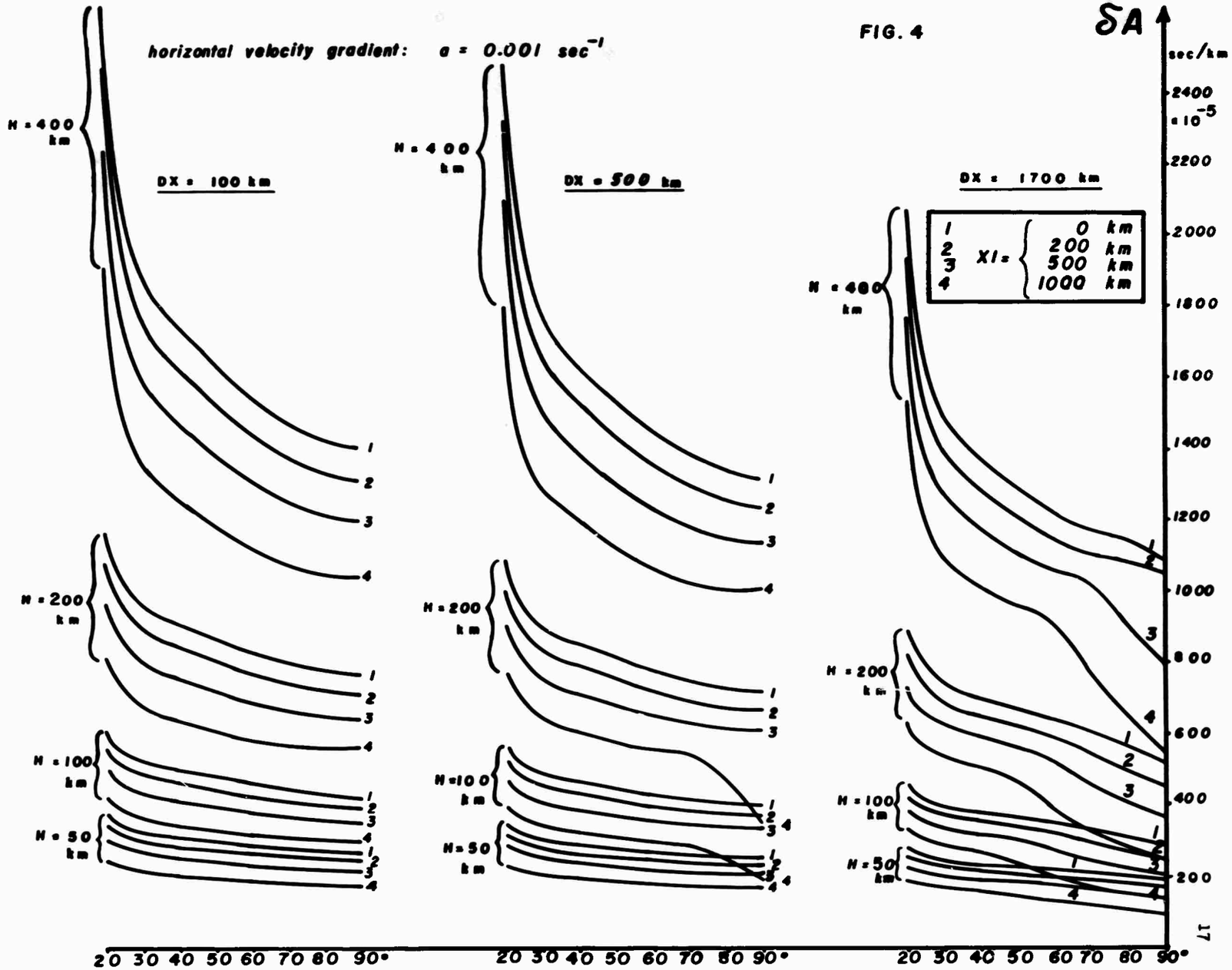
horizontal velocity gradient: a = 0.001 sec⁻¹
δA
sec/km
DX = 100 km
DX = 500 km
DX = 1700 km
H = 400 km
H = 200 km
H = 100 km
H = 50 km
1 XI = 0 km
2 200 km
3 500 km
4 1000 km
2400
2200
2000
1800
1600
1400
1200
1000
800
600
400
200
20 30 40 50 60 70 80 90°

glaciations of Fennoscandia. The extent of the anomaly suggests that the portions most heavily glaciated suffered a compression of the strata. The removal of the ice resulted in an elastic, instantaneous rebound and an imperfect elastic rebound not completed yet, as revealed by the present continental uplift of Fennoscandia.

This interpretation of the continental uplift as time-dependent dilatation is even more plausible, as newer gravimetric observations in Fennoscandia are not in support of the once much favored interpretation of the uplift as isostatic readjustment. A recently published map of isostatic gravity anomalies for Sweden does not indicate any mass deficit under the country, as required for the latter interpretation. On the other hand, the interpretation of the uplift as dilatation is in agreement with these seismological observations as much as it is with known gravimetric, geological and mareographic data.

S-time delays.

This travel-time study is of special interest in connection with the establishment of a seismic array station in Norway under Project VELA-Uniform. The work on P-times is essentially completed and it will be supplemented with a corresponding study of the S-times. Some work has been performed already.

The P-times used in the study were reported in the bulletins usually with an accuracy to 0.1 sec. The S-times are usually reported with an accuracy of only 1.0 sec. Moreover, the identification of the S-phase is more difficult, which leads eventually to systematic errors in the S-times. From this it is evident that in order to obtain statistically significant

data a larger amount of data must be used, besides the elimination of systematically errant observations.

Arrival times of S-waves at 16 Scandinavian stations from more than 1200 earthquakes have been collected. Several computer programs for the calculation of relative S-time delays, slopes of the S-travel time curve and related quantities have been adapted or prepared and test-run. Work on this problem is under progress.

3. S Wave Studies

All studies of S waves carried out in the past year under this contract had the purpose of determining the crust and mantle velocity distribution and its regional variations. This information is required for the accurate location of seismic events and the determination of their magnitude, as well as for predicting the travel time and amplitudes of seismic waves which result from a hypothetical earthquake or explosion.

The S wave studies may be divided into three parts: travel times and amplitudes of S generated by nuclear explosions and earthquakes as recorded by seismograph stations throughout North America, apparent wave slownesses ($dT/d\Delta$) of S waves across LASA, and studies of the spectral properties of the S-wave ground motion and their relation to crustal structure.

Travel Times and Amplitudes.

During the twelve-month period covered by this report work was completed on travel-time and amplitude studies of S for a surface focus as recorded in North America at distances of 1700 to 6800 km. This work complements earlier determinations of observational travel times for the same distances for focal depths of 33 and 120 km. By making use of all three travel-time curves

we have calculated an S wave velocity model for the upper 1500 km of the mantle which is representative of an "average United States" mantle structure. These data establish the existence of a low-velocity channel at a depth of 150 to 200 km, a discontinuous velocity increase at 400 km depth, and a large but continuous velocity increase at 750 km. The velocity gradients are almost zero in the depth intervals 50 to 150, 250 to 350, and 500 to 700 km. Some of the data appear to demand in addition the existence of secondary low-velocity channels at depths of 340 to 370 and 670 to 710 km, although the evidence is not conclusive. In an attempt to resolve this important question data which will make possible the construction of observational travel-time curves of S, sS and ScS for a focal depth of 600 km are being gathered. Data extending the travel-time curves of S for depths of 33 and 120 km to distances beyond 10,000 km for the purpose of obtaining lower mantle velocity information are also being accumulated.

Figure 5 compares the travel-time curve developed in this research and velocity model (I.N.2) with those of Anderson and his colleagues at the California Institute of Technology (CIT 11GB). The solid line curve results directly from observations of the travel time of the S phase for a surface focus. From this the I.N.2 velocity model is deduced. The CIT 11GB velocity model, on the other hand, is calculated from the observed dispersion of surface waves. Then from this velocity model, shown in the figure by dashed lines, the dashed-line travel-time curve is computed (Julian and Anderson, 1968). The overall agreement between the two travel-time curves is considered to be remarkably good except for the branches AB and BC, where the large discrepancies are

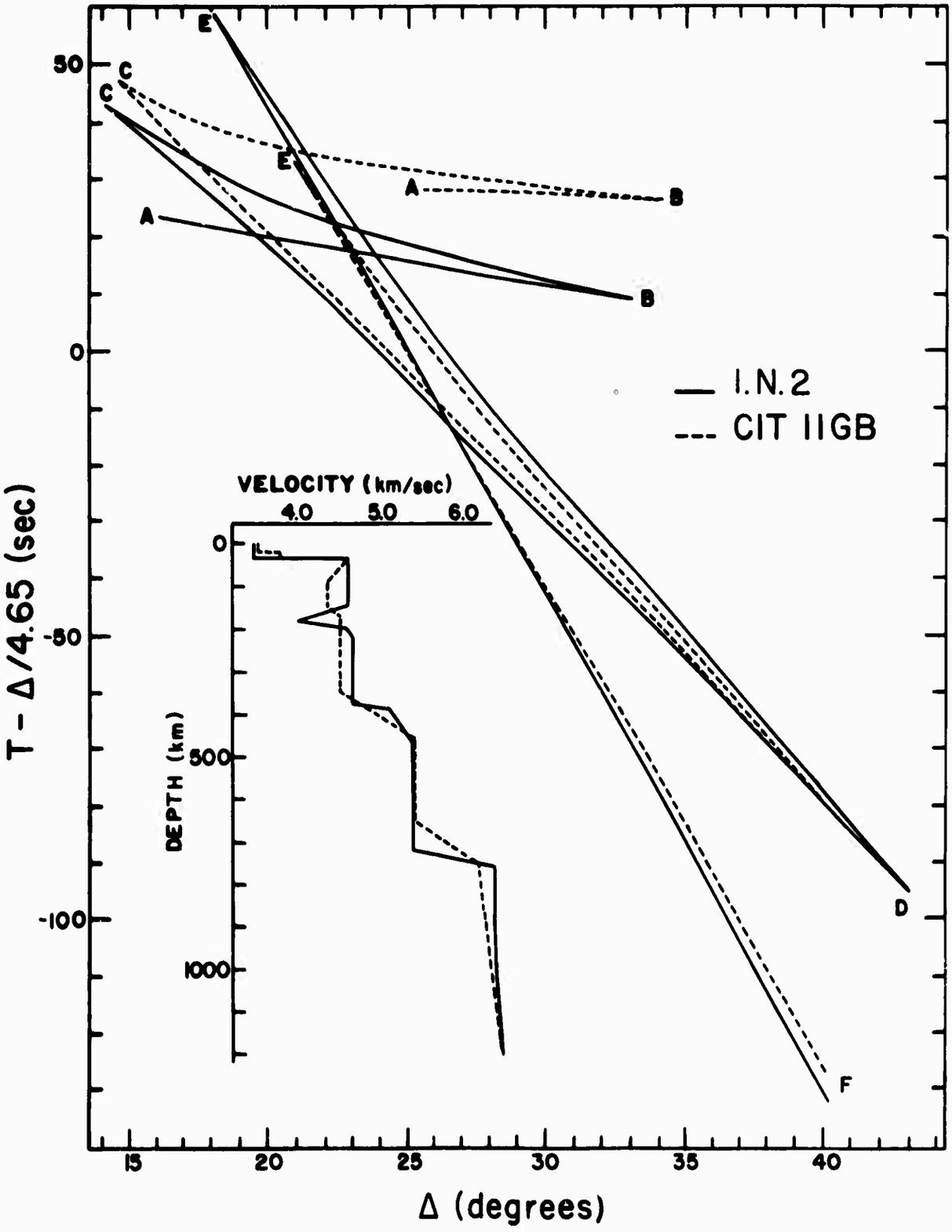
T - Δ/4.65 (sec)
Δ (degrees)
50
0
-50
-100
15
20
25
30
35
40
E
C
C
E
A
B
A
B
D
F
— I.N.2
--- CIT 11GB
VELOCITY (km/sec)
4.0
5.0
6.0
0
500
1000
DEPTH (km)

Figure 5

caused by a different depth to the low-velocity channel.

It should be noted that our travel-time curve of S from nuclear explosion data is the first of its kind. The techniques which make the identification of S possible, namely resolution into SH and SV components and the use of particle motion diagrams, were developed in earlier VELA-Uniform work done by us.

S wave amplitude data from the Nevada explosions GREELEY and HALF BEAK were used for three purposes, namely: 1) to distinguish between a discontinuity in velocity and in velocity gradient at depths of about 400 and 750 km in the mantle, 2) to estimate the magnitude of the nuclear explosions from the S wave data, and 3) to study the pattern of radiation of seismic energy from the explosions.

Relatively large amplitudes were observed near point E of the travel-time curve, but there was no increase in amplitude near D (see Fig. 5). This suggests that the velocity increase beginning at 750 km depth is continuous, but that the velocity gradient is discontinuous (Bullen, 1961). There is no indication of an amplitude increase near points B and C, which indicates that the velocity increase at 400 km depth is discontinuous.

Differences in the magnitudes determined from P wave amplitudes and from Rayleigh wave amplitudes are presently considered to be an important discriminant between earthquakes and explosions. Additional magnitude estimates, based on S wave amplitudes, may be of help in such discrimination. From our amplitude measurements of S we determined the magnitude of HALF BEAK to be 4.9, with a range of values of 4.5 to 5.2 and a standard deviation of 0.2. For GREELEY the average S wave magnitude was 5.3, with

a range of 4.8 to 5.8 and a standard deviation of 0.2. Magnitude determinations for these are summarized in Table 1.

Table 1

Event	Magnitude P wave	S wave	Surface wave
HALF BEAK	6.02 ± 0.60 (Teledyne)	4.9 ± 0.2 (St. Louis U.)	
	6.2 (Uppsala)		
GREELEY	6.29 ± 0.45 (Teledyne)	5.3 ± 0.2 (St. Louis U.)	5.6 (Eskdalemuir)
	6.4 (Uppsala)		
	6.1 (Eskdalemuir)		

Note that for GREELEY the S wave magnitude is 0.3 units lower than the surface wave magnitude, and that for both HALF BEAK and GREELEY the S wave magnitude is a whole unit smaller than the P wave magnitude. For earthquakes, on the other hand, the P and S wave magnitudes are the same, after the effects of the radiation pattern have been considered. Thus relatively small amplitude S waves, compared to P, are suggestive of an explosion. This observation in itself is of not much importance in the nuclear explosion detection problem because only very large explosions generate S waves. But the converse may be of value, i.e., <u>any event for which the S wave magnitude is as large or larger than the P wave magnitude must be an earthquake</u>.

The radiation patterns for both HALF BEAK and GREELEY were similar for the SH arrivals of branches AB and EF and the horizontal SV arrivals of branch EF, which taken together constitute most of the S arrivals. The SV arrivals were all positive

(towards the epicenter) whereas the SH arrivals were counter-clockwise as viewed from the epicenter for stations to the northwest, north, and north-northeast and clockwise for stations to the east-northeast, east, and east-southeast. The radiation pattern of SH, considered together with the observation that the first P motion appeared as a compression at all distances and azimuths, indicates that the focal mechanism can be represented by a composite of a uniform compression and a double couple. Toksoz and Clermont (1967), using surface wave and P wave amplitudes, found a similar kind of mechanism for BILBY. If one assumes that the forces of the double couple lie in a horizontal plane, the direction of the predicted SH nodal line for BILBY based on their Rayleigh and P wave study agrees with that observed for HALF BEAK and GREELEY. This leads to the conclusion that the radiation pattern for all these events is similar, even though the distance separating the shot points is as much as fifty km and BILBY was in tuff, HALF BEAK in rhyolite, and GREELEY in zeolitized tuff.

dT/dΔ of S waves across LASA.

Develecorder records of the long period seismographs of the D and F rings at LASA were used to obtain dT/dΔ values for the S waves across the array. The records of twelve earthquakes, whose hypocentral coordinates are listed in Table 2, were digitized and then resolved into SH and horizontal SV components of motion. Arrival times were read of the onset and the first peak or trough of the SH motion. The waveforms at the various stations generally were consistent, so that both peaks and onsets gave the same value of dT/dΔ. Particle motion diagrams were

used for those cases in which the onset times could not reliably be determined from the SH component directly.

Table 2

Date	Origin time	Lat.	Long.	Depth	Magn.
1 May 67	07-09-00.5	39.7 N	21.3 E	15 km	5.6
9 May 67	12-36-36.8	56.6 N	152.6 W	33	5.0
11 May 67	15-05-16.8	20.3 S	68.5 W	67	6.1
13 May 67	05-18-55.4	56.5 N	152.6 W	33	5.3
16 May 67	12-58-09.5	13.5 N	90.6 W	95	4.8
21 May 67	07-18-12.8	27.9 N	111.3 W	33	4.7
27 May 67	17-22-58.7	51.9 N	176.1 E	34	5.8
19 Jun 67	17-07-45.4	52.7 N	166.9 W	33	5.7
15 Nov 67	21-31-51.5	28.7 S	71.2 W	15	6.2
17 Nov 67	04-58-56.8	28.5 N	43.8 W	33	5.2
23 Nov 67	13-42-01.6	80.2 N	1.0 W	10	5.8
1 Dec 67	13-57-02.4	49.5 N	154.4 E	136	5.9

The values of $dT/d\Delta$, together with distance to the center of the array, are presented in Table 3. Also included are the values of dT and $d\Delta$ between pairs of stations, and the value of $dT/d\Delta$ from the Jeffreys-Bullen tables for the appropriate distance and focal depth. If $d\Delta$ is of the order of 100 km, an error of 1 sec in dT will produce an error of about 0.01 sec/km in $dT/d\Delta$. The latter figure corresponds to about a 10% error, because for teleseismic distances $dT/d\Delta$ varies from about 0.15 to 0.07 sec/km. This example illustrates the importance of an accurate determination of the quantity dT.

Accurate determinations of dT require an adequate sampling rate. In digitizing the Develocorder records we sampled approximately four points per second, which is a minimum acceptable number for such a study. One point per second, for example, is certainly inadequate. Because the waveforms of S were consistent across the array, we were able to estimate dT to the nearest

0.1 sec by using interpolation. In general, the most reliable values of $dT/d\Delta$ are those for which $d\Delta$ is the largest. Only those station pairs for which $d\Delta$ is greater than 100 km are listed in Table 3.

Table 3

Date	(°)	Station Pair	dT (sec)	$d\Delta$ (km)	$dT/d\Delta$ (km/sec)	$dT/d\Delta_{avg}$ (km/sec)	$dT/d\Delta_{J-B}$ (km/sec)
1 May 67	82.0°	F1-F3	18.1	211.89	0.085		
		F3-F4	10.7	132.73	0.081		
						0.083	0.092
9 May 67	29.9	D2-F4	16.8	116.97	0.143		
		D4-F2	18.1	124.17	0.146		
		F2-F4	27.1	189.22	0.143		
						0.144	0.142
11 May 67	74.8	D2-F4	12.9	123.46	0.104		
		D4-F2	14.2	133.40	0.106		
		F2-F4	21.5	200.72	0.107		
						0.106	0.100
13 May 67	29.9	D2-F4	17.2	116.84	0.147		
		D4-F2	18.1	123.98	0.145		
		F2-F4	27.5	188.98	0.145		
						0.146	0.142
16 May 67	35.6	D2-F4	17.6	122.25	0.144		
		D4-F2	16.8	135.53	0.126		
		F2-F4	26.6	199.44	0.133		
						0.134	0.138
21 May 67	19.1	D1-F3	21.9	114.91	0.190		
		D2-F1	21.5	109.54	0.196		
		D3-F1	21.1	113.21	0.186		
		D4-F3	22.3	116.88	0.191		
		F1-F2	31.4	162.45	0.193		
		F1-F3	35.7	185.95	0.191		
		F2-F4	27.1	135.39	0.199		
		F3-F4	31.4	158.89	0.197		
						0.193	0.201
27 May 67	48.7	D2-F4	14.6	116.87	0.125		
		D4-F2	16.3	123.86	0.131		
		F2-F4	24.1	188.90	0.128		
						0.128	0.125
19 Jun 67	38.7	D2-F4	16.3	113.38	0.144		
		D4-F2	15.9	119.66	0.132		
		F2-F4	25.8	183.09	0.140		
						0.139	0.136
15 Nov 67	81.4	D2-F4	14.9	123.16	0.121		
						0.121	0.093
17 Nov 67	51.3	D3-F1	11.1	101.30	0.109		
		F1-F3	18.3	150.98	0.121		
		F1-F4	17.1	132.49	0.128		
		F2-F3	16.2	123.32	0.131		
						0.122	0.124

Date	Δ (°)	Station pair	dT (sec)	d$\sim$ (km)	dT/d$\sim$ (km/sec)	dT/dΔ avg (km/sec)	dT/dΔ J-B (km/sec)
23 Nov 67	46.9	D3-F1	14.0	111.39	0.125		
		F1-F2	20.4	163.44	0.124		
		F2-F4	17.5	137.45	0.127		
						0.125	0.128
1 Dec 67	61.5	D2-F4	13.2	120.74	0.109		
		D4-F2	14.1	128.93	0.109		
		F2-F4	22.6	195.58	0.115		
						0.111	0.113

Comparison of the observed and calculated values of dT/dΔ shows good agreement out to 60°, with the difference between values always less than 5%. There are an insufficient number of data to look for any azimuthal dependence such as has been found for the dT/dΔ of P waves across LASA. However, we plan to continue this work as additional usable data become available and hope to be able to acquire enough data to investigate the effect of azimuth.

Spectral Properties of Ground Motion.

The theory that predicts the character of the spectra of the components of the S wave ground motion, which depends on earth structure, angle of incidence, and wave frequency, has been developed by Haskell (1960, 1962) and Nuttli (1964). The predicted amplitude vs frequency relation for SV is especially interesting because it indicates that there are large changes in amplitude with small changes in frequency and/or angle of incidence for particular values of the angle of incidence and frequency. However, none of these features have been verified by observation. The purpose of this research is to obtain S wave spectra from the observational data and to compare some of their properties with those expected from theory.

Seismograms of five earthquakes have been analyzed. Table 4 lists their dates and hypocentral coordinates. The long period

Table 4

Earthquake Number	Date	Origin Time	Lat.	Long.	Depth	Magn.
1	13 Apr 63	02-20-57.9	6.26°S	76.66°W	125 km	6 3/4-7
2	15 Oct 63	09-59-30.1	67.20 N	18.40 W	33	5½
3	12 Jan 64	06-00-13.2	53.20 N	166.30 W	33	5½
4	28 Jun 64	17-27-59.8	4.00 N	32.40 W	33	5.3
5	18 Sep 64	13-12-42.3	39.80 N	29.70 W	20	5½

seismograms used are from LRSM stations at epicentral distances of 50° to 70°. Table 5 shows the stations used for each event, their epicentral distances, and back azimuths.

Table 5

Earthquake Number	Station	Distance	Azimuth (station to epicenter)
1	DHNY	48.23°	182.15°
	DRCO	52.33	139.29
	FMUT	55.97	135.56
	LCNM	47.90	137.78
	NGWS	52.76	165.39
	PMWY	54.08	143.66
	SEMN	52.97	157.15
	TFCL	58.01	126.25
	WNSD	53.70	150.28
2	AZTX	55.44	28.05
	BLWV	45.36	29.19
	RTNM	55.22	28.25
	SKTX	55.14	28.06
3	DRCO	56.62	68.77
	FRMA	52.99	75.25
	GIMA	51.24	77.40
	JUTX	54.24	66.34
4	BRPA	55.04	118.11
	BLWV	55.83	114.66
	DRCO	75.99	95.76
	LSNH	53.04	127.39
5	DRCO	59.15	61.40
	JELA	50.28	62.49
	RTNM	57.09	62.25
	RYND	50.62	71.22
	WNSD	51.45	68.22

In order to obtain the spectral components of S we employed the following procedure. The seismograms were digitized

at an 0.5 sec interval, and the horizontal components of motion resolved into components along (U_R) and transverse to (U_T) the great circle path at the station. The average length of seismogram digitized corresponded to about forty seconds of time. Because S is followed closely by other phases such as sS and PS, the data were passed through a Hamming lag window to suppress the effect of these later phases. After reductions for the frequency response of the seismograph system were made, the data were Fourier analyzed using a technique known as Filon's method.

The results to date of the analysis can best be presented in the form of some typical examples. Theoretical curves of the spectral ratio FR/FZ were prepared for the Haskell and McEvilly crustal models (see Table 6 for properties) for angles of incidence between 20° and 36° in 2° steps. Curves of these spectral ratios were also prepared for a modified Haskell model, in which the crustal velocities were changed to $\alpha = 6.6$ km/sec and $\beta = 3.86$ km/sec.

Table 6

Model	Layer thickness (km)	Comp. wave velocity (km/sec)	Shear wave velocity (km/sec)	Density (gm/cm^3)
Haskell	37.0	6.285	3.635	2.869
	infinite	7.960	4.600	3.370
McEvilly	1.0	4.40	2.50	2.70
	10.0	6.10	3.50	2.70
	9.0	6.30	3.66	2.80
	18.0	6.60	3.86	2.90
	infinite	8.15	4.70	3.30

In discussing the plots of the spectral ratios we shall use the terms "character" and "shift" as defined by Hannon (1964). "Character" refers to the general shape of adjacent peaks and troughs of the spectral ratio curves. One curve is "shifted"

with respect to the other when segments of the curves having similar character are displaced with respect to the frequency coordinate.

Figure 6 presents the ratio FR/FZ of the amplitude spectra for earthquake number 1 at the station FMUT, as well as a theoretical curve for McEvilly's earth model for an angle of incidence of 34°. The left part of both curves (frequencies less than 0.18 cps) shows the same character. The difference in amplitudes of the curves can be reduced by decreasing the velocity contrast between the half space and the lowest crustal layer in the theoretical model. Better agreement between the theoretical and observed curves also might be obtained by a slight increase in total crustal thickness of the theoretical model.

Observed and theoretical spectral ratio curves of FR/FZ at TFCL, also for earthquake number 1, are given in Fig. 7. The angle of incidence, 34°, is the same as for Fig. 6, which is expected because both stations are at about the same epicentral distance. The modified Haskell's model gives a theoretical curve which has the same character as the observed one. The different levels of amplitude indicate that further adjustments are still required in the velocities of the theoretical model. A shift of the theoretical curve to the left is also needed.

Figure 8 contains spectral ratios of the station BRPA for earthquake number 4. The best fitting theoretical curve is for an angle of incidence of 32°, less than that of Figs. 6 and 7, which can be explained by the fact that the focal depth of earthquake number 1 is the greater. A change in amplitude, which can be produced by changing the velocities of the model, is required.

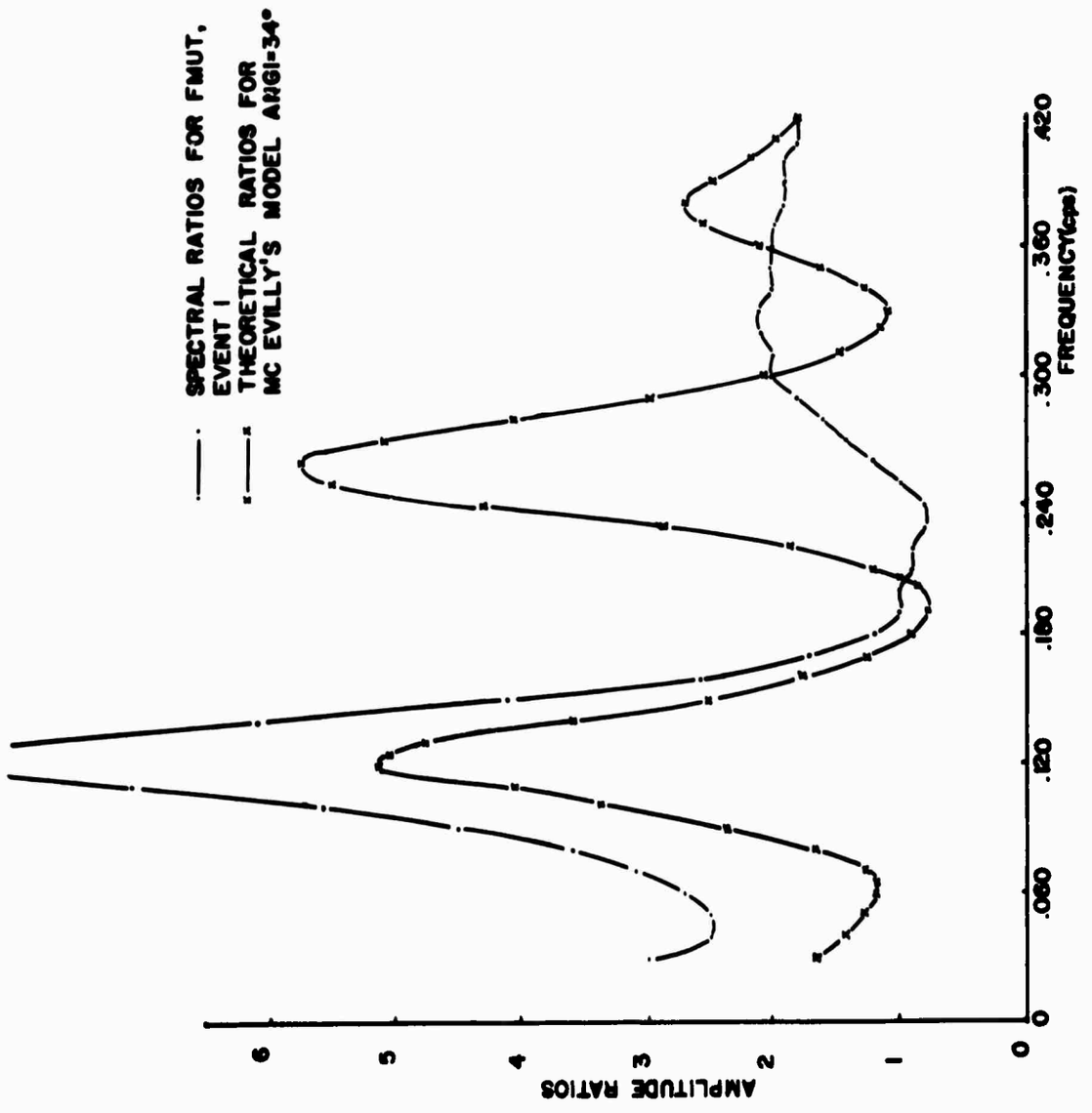
SPECTRAL RATIOS FOR FMUT, EVENT I
THEORETICAL RATIOS FOR MC EVILLY'S MODEL ANGI=34°
AMPLITUDE RATIOS
0
1
2
3
4
5
6
0
.060
.120
.180
.240
.300
.360
.420
FREQUENCY(cps)

Figure 6

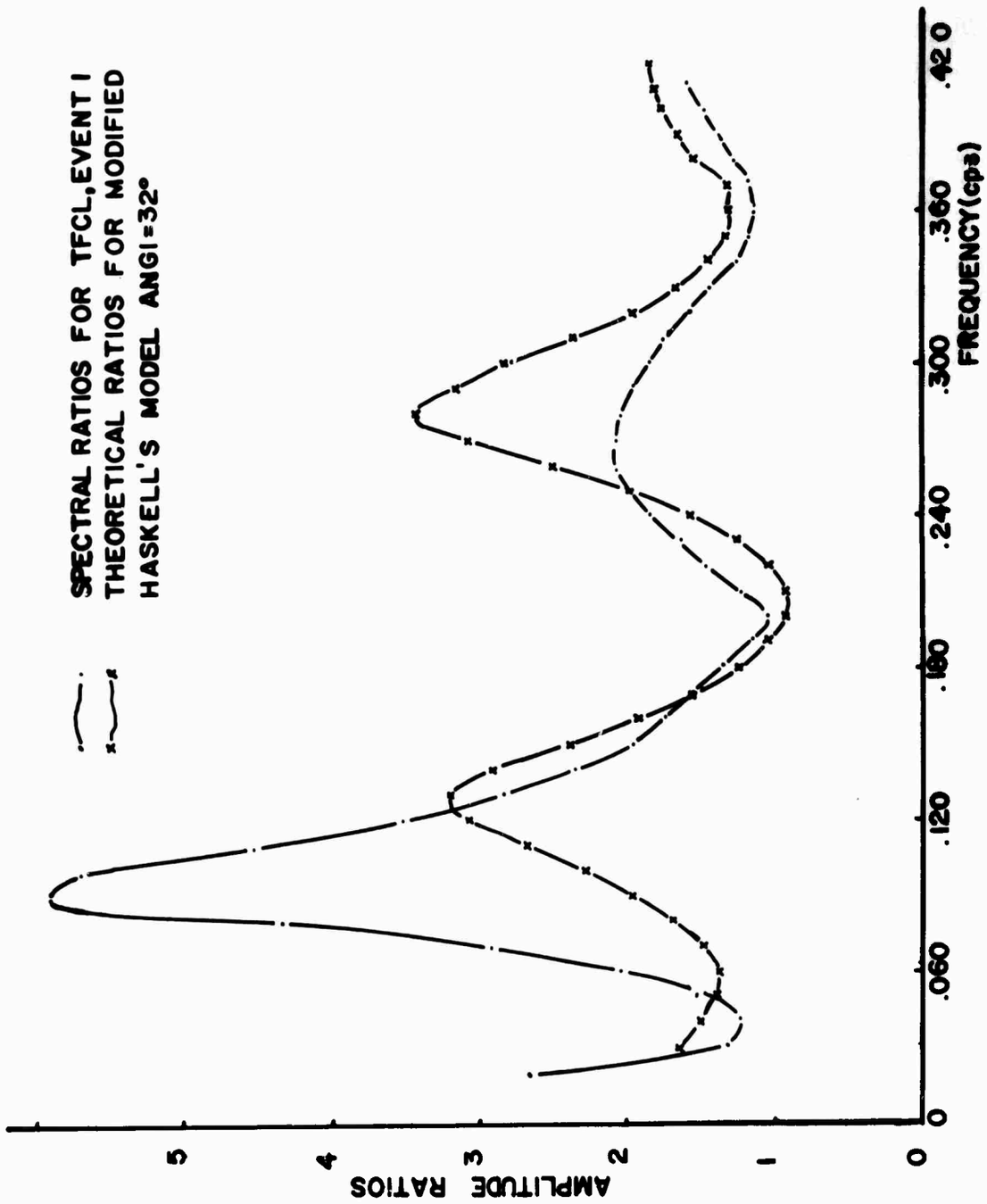
SPECTRAL RATIOS FOR TFCL, EVENT I
THEORETICAL RATIOS FOR MODIFIED
HASKELL'S MODEL ANGI=32°
AMPLITUDE RATIOS
0
1
2
3
4
5
0
.060
.120
.180
.240
.300
.360
.420
FREQUENCY(cps)

Figure 7

The observed spectral ratio curve of LSNH for earthquake number 4 (Fig. 9) has the position of the peaks and troughs interchanged as compared to those of Fig. 8. This is surprising, because both stations are approximately at the same distance and might be expected to have the same crustal structure.

Figure 10 is unusual in the sense that the best fit for RTNM for earthquake number 5 is found to be McEvilly's model with an angle of incidence of only 28°. The agreement in character of the observed and theoretical curves is fairly good, although the theoretical curve should be shifted slightly to the left.

In the previous discussion the best fitting theoretical curve was taken to be one of a set of curves for the McEvilly or Haskell models at angles of incidence of 20, 22, 24, 26, 28, 30, 32, 34, 35 and 36 degrees. It is apparent that none of these theoretical curves gives an ideal match to any of the observed curves. Better agreement can be had by changing the parameters of the earth model used to compute the theoretical curves. Further effort will be devoted to finding a systematic way of changing the parameters so as to get a better fit, such as by using partial derivatives of the spectral ratio with respect to the various parameters.

References

Bullen, K. E. (1961) "Seismic ray theory," Geophys. J., Roy. Astro. Soc., 4, 93-105.

Hannon, W. J. (1964) "An application of the Haskell-Thomson matrix method to the synthesis of the surface motion due to dilatational waves," Bull. Seism. Soc. Am., 54, 2067-2080.

Haskell, N. A. (1960) "Crustal reflection of plane SH waves," J. Geophys. Res., 65, 4147-4150.

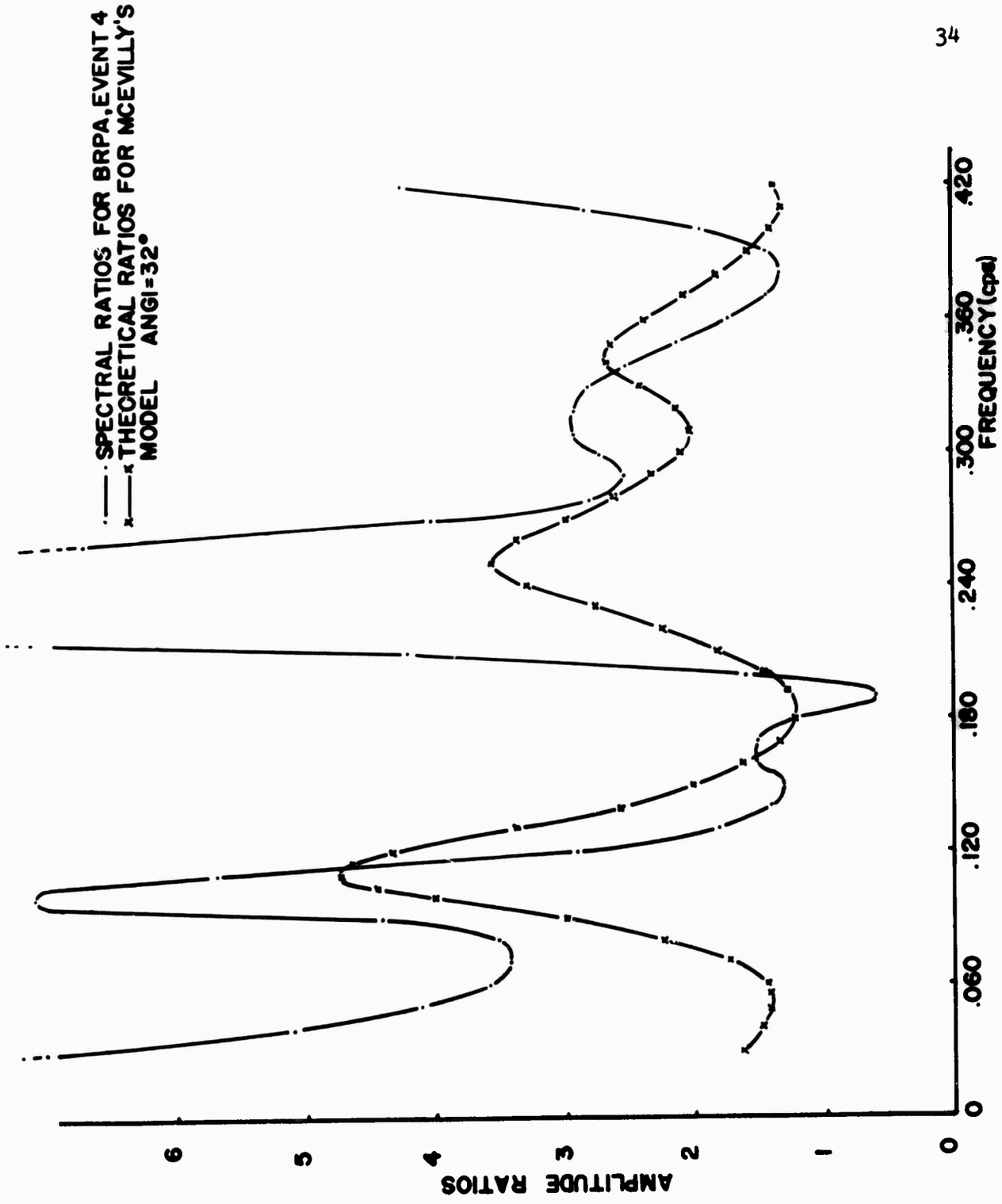
SPECTRAL RATIOS FOR BRPA, EVENT 4
THEORETICAL RATIOS FOR MCEVILLY'S MODEL ANGI=32°
AMPLITUDE RATIOS
FREQUENCY(cps)
0
1
2
3
4
5
6
.060
.120
.180
.240
.300
.360
.420

Figure 8

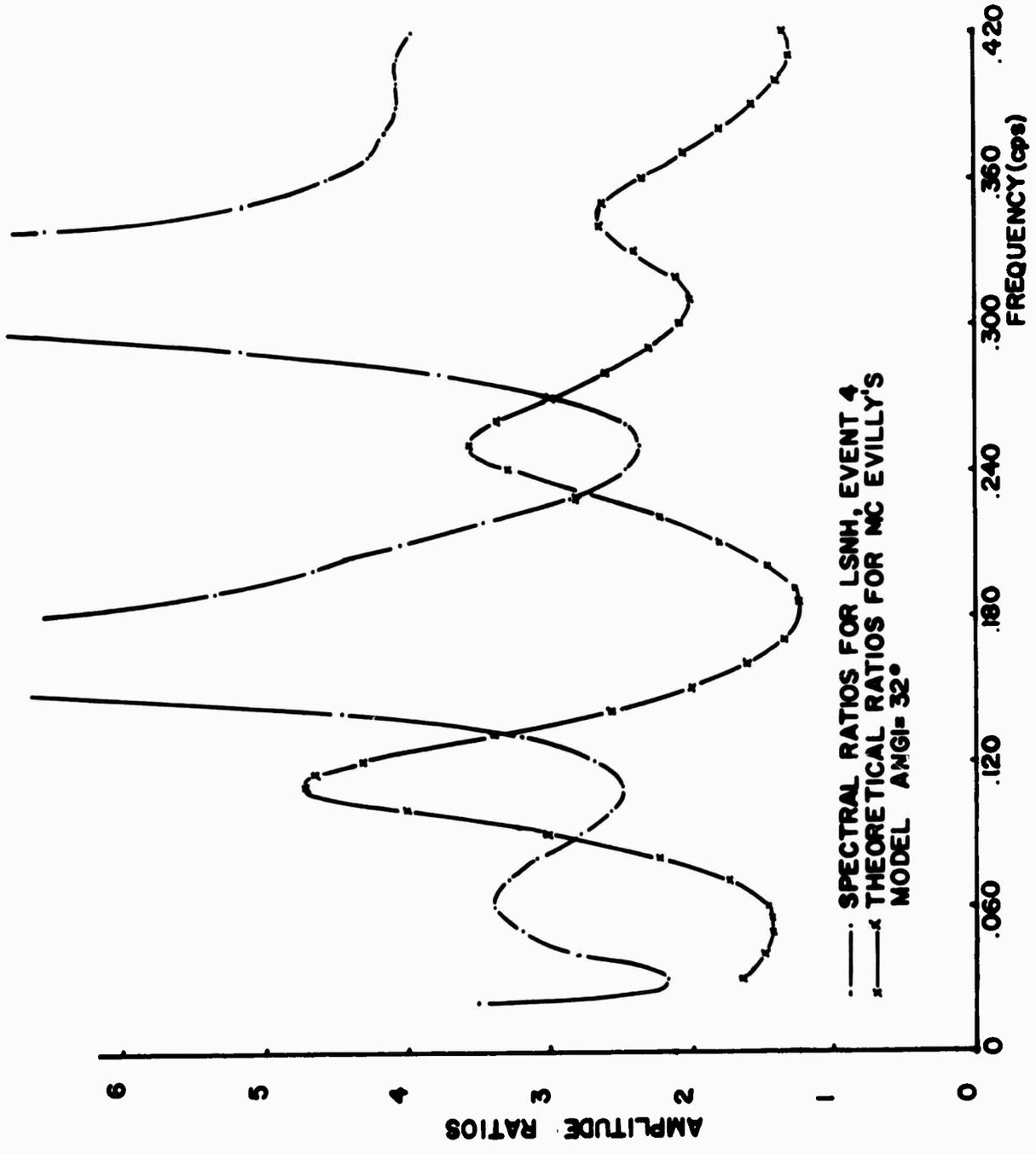
AMPLITUDE RATIOS
0
1
2
3
4
5
6
FREQUENCY(cps)
0
.060
.120
.180
.240
.300
.360
.420
SPECTRAL RATIOS FOR LSNH, EVENT 4
THEORETICAL RATIOS FOR MC EVILLY'S
MODEL ANGI= 32°

Figure 9

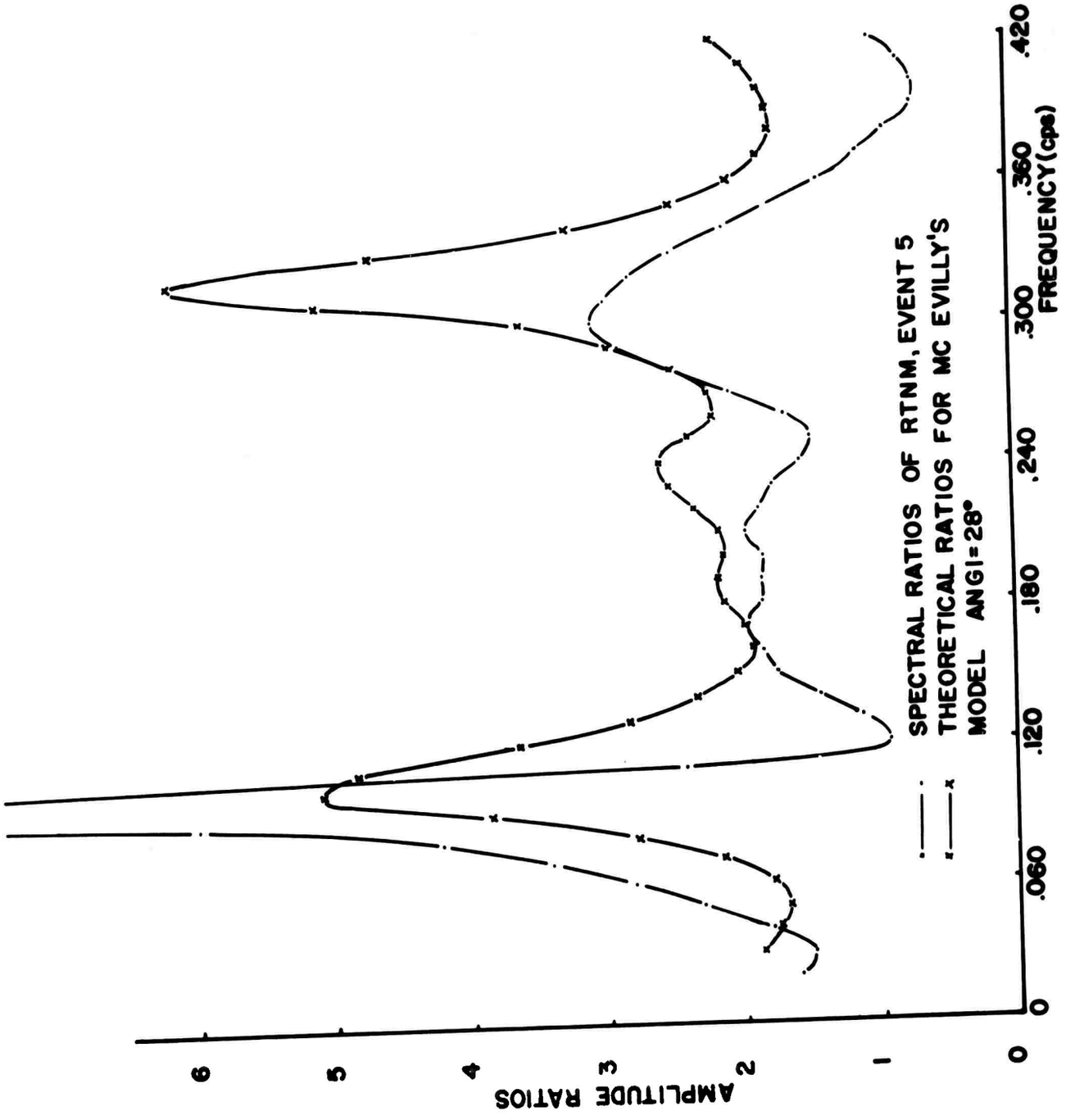
SPECTRAL RATIOS OF RTNM, EVENT 5
THEORETICAL RATIOS FOR MC EVILLY'S MODEL ANGI=28°
AMPLITUDE RATIOS
FREQUENCY(cps)
0
1
2
3
4
5
6
.060
.120
.180
.240
.300
.360
.420

Figure 10

Haskell, N. A. (1962) "Crustal reflection of plane P and SV waves," J. Geophys. Res., 67, 4751-4767.

Julian, B. R., and D. L. Anderson (1968) "Travel times, apparent velocities and amplitudes of body waves," Bull. Seism. Soc. Am., 58, 339-366.

Nuttli, O. W. (1964) "The determination of S-wave polarization angles for an Earth model with crustal layering," Bull. Seism. Soc. Am., 54, 1429-1440.

Toksoz, M. N., and K. Clermont (1967) Radiation of seismic waves from the BILBY explosion. Report prepared for AFTAC Washington, D.C.

4. Earthquake Energy Determination

The present method of energy determination from the magnitude-energy relations of Gutenberg and Richter or others is not very accurate. With the advent of the modern high-speed electronic computers, with the better understanding of focal mechanism of earthquakes and Q of the earth, with the knowledge of well-determined crustal structure and the existence of highly sensitive standard seismographs with well-determined instrumental response characteristics, it is now possible for us to take into account the various factors affecting the ground motion and to come up with more accurate energy estimates than it was possible in Gutenberg's time.

The seismogram can be visualized as the output of a series of filters into which an original seismic impulse has been fed. Each filter corresponds to a portion of the propagating medium and is characterized by a complex transfer function $H(\omega)$, which operates on the input spectrum and modifies it as it passes through. The final output of this filter series is $F(\omega)$, which is measurable at the surface. These complex functions may be written in terms of real amplitude and phase spectrums:

$$S(\omega) = A_o(\omega)\, e^{i \phi_o(\omega)} \qquad (1)$$

$$F(\omega) = A(\omega) e^{i \phi(\omega)} \qquad (2)$$

$$H_D(\omega) = A_D(\omega) e^{i \phi_D(\omega)} \qquad (3)$$

and similarly for $H_{CR}(\omega)$ and $H_{INS}(\omega)$, where $H_D(\omega)$, $H_{CR}(\omega)$, $H_{INS}(\omega)$ are the complex transfer functions of the mantle, crust and the seismograph. It then follows from the definition of the transfer function that

$$A_o(\omega) = A(\omega) / \left[A_{INS}(\omega)\, A_{CR}(\omega)\, A_D(\omega) \right] \qquad (4)$$

$$\phi_o(\omega) = \phi(\omega) - \left[\phi_{INS}(\omega) + \phi_{CR}(\omega) + \phi_D(\omega) \right] \qquad (5)$$

where $A(\omega)$ and $\phi(\omega)$ are known from the observed body wave data.

A program has been written for obtaining discrete Fourier transforms from the digitized data of the pulse recorded on the seismogram. An existing program has been adapted for obtaining the steady state harmonic response of the seismograph. There is provision for introducing magnification values at five frequencies in the input data and the response for any intermediate frequency is obtained by linear interpolation. A program based on the Haskell-Thomson matrix formulation for obtaining the crustal response for incident P and S waves, as a function of frequency and angle of incidence, was tested.

As in Teng and Ben-Menahem (1965), the amplitude response for the effect of geometrical spreading and absorption in the mantle may be expressed as

$$A_D(\omega) = G \times AT(\omega) \qquad (6)$$

where

$$G = \frac{1}{r_o} \left[\frac{\sin i_h}{\cos i_o \sin \theta} \frac{di_h}{d\theta} \right]^{1/2} \qquad \theta = \frac{\Delta}{r_o} \qquad (7)$$

is a factor due to geometrical spreading and $AT(\omega)$ is the attenuation function. Assuming a Bullen A velocity model and a Q(H) model calculated by Anderson and Archambeau (1964), Teng and Ben-Menahem obtain the expression for the attenuation function as follows:

$$AT(\omega) = \exp\left[-\int_{ray} \frac{\omega\, ds}{2Q(r)\, v(r)}\right]$$

$$\approx \exp\left[-\omega \frac{r_o}{v_o} \left| \frac{\sin(i_h - i_o)}{\sin i_h} \right| \times 10^{-3}\right] \qquad (8)$$

where the subscripts o and h refer to the base of the crust and the source level, respectively. A program has been prepared to correct for the effect of geometrical spreading and absorption in the mantle and reduce it to the focal sphere.

Let (x,y,z) be the coordinates of a point in a right-handed coordinate system X, Y, Z related to the orientation of the source mechanism, let $(\bar{x},\bar{y},\bar{z})$ be the coordinates of the same point in a geographic coordinate system (N, E, and down) referred to the origin of the focal sphere, and let $(\alpha_x, \beta_x, \gamma_x)$ and $(\alpha_y, \beta_y, \gamma_y)$ be the direction cosines of the X and Y axes with respect to $\bar{x}$, $\bar{y}$, $\bar{z}$. Then the displacement field due to a double couple source with forces oriented along the X and Y axes is given by (see e.g., Bessonova et al, 1960)

$$u_a = \frac{2}{4\pi\rho} \frac{x}{a^3} \frac{y}{R^3} k'\left(t-\frac{R}{a}\right) \qquad (9)$$

$$u_b^H = -\frac{1}{4\pi\rho} \frac{C}{b^3 R^3} k'\left(t-\frac{R}{b}\right) \qquad (10)$$

$$u_b^P = \frac{1}{4\pi\rho} \frac{D}{b^3 R^3} k'\left(t-\frac{R}{b}\right) \qquad (11)$$

where u_a is the radial motion of the P wave, u_b^H and u_b^P are the SH and SV components, respectively, a and b are the velocities

of P and S waves, respectively, R is the radial distance to the point of observation and

$$C = \frac{(\alpha_x y + \alpha_y x)\,\bar{y} - (\beta_x y + \beta_y x)\,\bar{x}}{\sin i_o} \qquad (12)$$

$$D = \frac{2xy \cos^2 i_o - \bar{z}\,(\gamma_x y + \gamma_y x)}{\sin i_o \cos i_o} \qquad (13)$$

Based on these formulae a program has been prepared for the P and S wave radiation pattern on the focal sphere as a function of the angle of incidence at the focus and azimuth, due to a double couple source of arbitrary orientation.

The next step is to develop a formula for the energy determination from the observed spectrum of body wave pulses and to combine the above programs. At a later stage the effect of the finiteness of the source and rupture velocity is planned to be incorporated in the energy formula. At present attention is concentrated on intermediate and deep focus earthquakes which give P and S pulses isolated from pP and sS, respectively. Later shallow earthquakes may be included. For these the effect of interference with the main pulse of crustal reverberations must be removed prior to analysis.

References

Anderson, D., and C. B. Archambeau (1964). The anelasticity of the earth, J. Geophys. Res., 69, 2071-2084.

Bessonova, E. N., O. D. Gotsadze, V. I. Keilis-Borok, I. V. Kirillova, S. D. Kogan, T. I. Kikhtikova, L. N. Malinovskaya, G. I. Pavlova and A. A. Sorskii (1960). Investigation of the mechanism of earthquakes, Trans. (TRUDY) of the Geophysics Inst. of the Akademy of Sci., USSR, 40, 1966. (English translation published by the American Geophysical Union.)

Haskell, N. A. (1953). The dispersion of surface waves on multilayered media, Bull. Seism. Soc. Am., 43, 17-34.

Teng, T.L., and A. Ben-Menahem (1965). Mechanism of deep earthquakes from spectrums of isolated body-wave signals, J. Geophys. Res., 70, 5157-5170.

5. The Effect of Focal Depth on the Spectrum of Body Waves.

As an approach to the problem of determining the focal depth of a seismic event from the spectrum of body waves, the following problem was considered: In a layered spherical earth a system of forces acts at a particular level. The problem is to determine how the ratio of the frequency spectrum of body waves recorded at a point on the surface of the sphere to the frequency spectrum of the system of forces at the source level is influenced by the depth of the layer at which the force system acts. This problem was investigated for a layered sphere (having arbitrary number of layers and a liquid core) with arbitrary orientation of the system of forces, acting at one particular level. An analytical solution using Haskell-Thomson type of complex matrices was obtained. However, the numerical calculation even for the simplest kind of force distribution appeared very difficult, and the spherical earth model was put aside. The problem was reformulated for a layered flat earth model.

The system consists of (n-1) layers over a half-space. The free surface is labelled "0", and the i^{th} interface is the bottom of the i^{th} layer. The half-space is layer n. On the S^{th} interface a system of time-varying forces acts. The problem is to derive the amplitude of plane waves which propagate along a specified direction to a point in the interior of the system. This direction has a specified azimuth with respect

to the epicenter and a specified inclination with respect to the vertical at the focus.

Inside the half-space, at distances far away from the source layer, the wave propatation along the specified direction can be considered as equivalent to wave propagation along a ray path which is characterized by a particular azimuth and a particular ray parameter. Thus, the amplitude of plane waves of various frequencies which propagate in the half-space will give considerable information regarding the spectrum of body waves which one expects to record at a particular epicentral distance and at a particular azimuth for a spherical earth. In particular, it is possible to investigate how the amplitudes of plane waves of various frequencies are influenced by the depth of the layer on which the system of forces act. The formulation of the problem follows.

Mathematical formulation.

Displacement potentials are defined as

$$\vec{S}(u, v, w) = \text{grad}\,\varphi + \text{curl curl}(0,0,\psi) + \text{curl}(0,0,\Lambda) \qquad (1)$$

Equations of motion are satisfied if

$$\nabla^2\varphi = \frac{1}{\alpha^2}\frac{\partial^2\varphi}{\partial t^2}$$

$$\nabla^2\psi = \frac{1}{\beta^2}\frac{\partial^2\psi}{\partial t^2} \qquad (2)$$

$$\nabla^2\Lambda = \frac{1}{\beta^2}\frac{\partial^2\Lambda}{\partial t^2}$$

The displacements and stress are given by

$$
\begin{aligned}
u &= \frac{\partial}{\partial x} f_1(x,y,z) + \frac{\partial}{\partial y} f_5(x,y,z) \\
v &= \frac{\partial}{\partial y} f_1(x,y,z) - \frac{\partial}{\partial x} f_5(x,y,z) \\
w &= f_2(x,y,z) \\
p_{zx} &= \frac{\partial}{\partial x} f_3(x,y,z) + \mu \frac{\partial}{\partial y} f_6(x,y,z) \\
p_{zy} &= \frac{\partial}{\partial y} f_3(x,y,z) - \mu \frac{\partial}{\partial x} f_6(x,y,z) \\
p_{zz} &= f_4(x,y,z)
\end{aligned}
\tag{3}
$$

where f_1, f_2, f_3, f_4 are functions of φ and ψ and f_5 and f_6 are functions of Λ alone:

$$
\begin{aligned}
f_1(x,y,z) &= \varphi + \frac{\partial \psi}{\partial z} \\
f_2(x,y,z) &= K_\beta^2 \psi + \frac{\partial}{\partial z}\left(\varphi + \frac{\partial \psi}{\partial z}\right) \\
f_3(x,y,z) &= \mu\left[2\frac{\partial}{\partial z}\left(\varphi + \frac{\partial \psi}{\partial z}\right) + K_\beta^2 \psi\right] \\
f_4(x,y,z) &= -\lambda K_\alpha^2 \varphi + 2\mu \frac{\partial}{\partial z}(K_\beta^2 \psi) + 2\mu \frac{\partial^2}{\partial z^2}\left(\varphi + \frac{\partial \psi}{\partial z}\right) \\
f_5(x,y,z) &= \Lambda(x,y,z) \\
f_6(x,y,z) &= \frac{\partial}{\partial z} \Lambda(x,y,z)
\end{aligned}
$$

The potential Λ does not contribute to the vertical components of displacement and normal stress and thus represents SH waves. The potential φ represents P waves and ψ represents SV wave:. P and SV waves are considered together and SH waves separately.

P and SV Waves.

We consider plane wave solutions of equation (2) in the form

$$\varphi(x,y,z,t) = \frac{1}{2\pi} e^{-i\omega t} \iint_{-\infty}^{+\infty} \left[\phi_1(K_1,K_2) e^{irz} + \phi_2(K_1,K_2) e^{-irz} \right] e^{+i(K_1 x + K_2 y)} \, dK_1 \, dK_2$$

(4)

$$\psi(x,y,z,t) = \frac{1}{2\pi} e^{-i\omega t} \iint_{-\infty}^{+\infty} \left[\psi_1(K_1,K_2) e^{isz} + \psi_2(K_1,K_2) e^{-isz} \right] e^{+i(K_1 x + K_2 y)} \, dK_1 \, dK_2$$

where

$$r^2 + K_1^2 + K_2^2 = \omega^2/\alpha^2 = K_\alpha^2 \qquad (5)$$

$$s^2 + K_1^2 + K_2^2 = \omega^2/\beta^2 = K_\beta^2 \qquad (6)$$

The displacements and the stresses will be continuous across the various interfaces if the functions f_1, f_2, f_3, f_4 are continuous across these interfaces. Using eq. (4), the functions $f_1 \ldots f_4$ can be written as:

$$f_1(x,y,z) = \frac{1}{2\pi} \iint_{-\infty}^{+\infty} \left[\phi_1 e^{irz} + \phi_2 e^{-irz} + is(\psi_1 e^{isz} - \psi_2 e^{-isz}) \right] e^{+i(K_1 x + K_2 y)} \, dK_1 \, dK_2$$

$$f_2(x,y,z) = \frac{1}{2\pi} \iint_{-\infty}^{+\infty} \left[ir(\phi_1 e^{irz} - \phi_2 e^{-irz}) - s^2(\psi_1 e^{isz} + \psi_2 e^{-isz}) + K_\beta^2(\psi_1 e^{isz} + \psi_2 e^{-isz}) \right] e^{+i(K_1 x + K_2 y)} \, dK_1 \, dK_2$$

$$f_3(x,y,z) = \frac{1}{2\pi}\iint_{-\infty}^{+\infty} \mu\left[k_\beta^2\left(\psi_1 e^{isz} + \psi_2 e^{-isz}\right)\right.$$

$$\left. + 2\left\{ir\left(\phi_1 e^{irz} - \phi_2 e^{-irz}\right) - s^2\left(\psi_1 e^{isz} + \psi_2 e^{-isz}\right)\right\}\right] \cdot$$

$$e^{+i(K_1 x + K_2 y)}\, dK_1\, dK_2 \qquad (7)$$

$$f_4(x,y,z) = \frac{1}{2\pi}\iint_{-\infty}^{+\infty}\left[-\lambda K_\alpha^2\left(\phi_1 e^{irz} + \phi_2 e^{-irz}\right) + 2\mu K_\beta^2 is\left(\psi_1 e^{isz} - \psi_2 e^{-isz}\right)\right.$$

$$\left. - 2\mu r^2\left(\phi_1 e^{irz} + \phi_2 e^{-irz}\right) - 2\mu is^3\left(\psi_1 e^{isz} - \psi_2 e^{-isz}\right)\right]$$

$$e^{+i(K_1 x + K_2 y)}\, dK_1\, dK_2$$

Let us consider a surface Z = constant. On this surface $f_1(x, y, z)$ can be written as a two-dimensional Fourier expansion as follows:

$$f_i(x,y,z)\Big|_{Z = \text{constant}} = \frac{1}{2\pi}\iint_{-\infty}^{+\infty} F_i(K_1,K_2)\, e^{+i(K_1 x + K_2 y)}\, dK_1\, dK_2$$

(8) where

$$F_i(K_1,K_2) = \frac{1}{2\pi}\iint_{-\infty}^{+\infty} f_i(x,y,z)\Big|_{Z = \text{constant}}\, e^{-i(K_1 x + K_2 y)}\, dx\, dy$$

$(i = 1, 2, 3, 4)$

Functions $F_1(K_1 K_2)$ are functions which are defined on the sur-

faces Z = constant. From eqs. (7) and (8), one may write the matrix relation

$$\begin{vmatrix} F_1(K_1,K_2) \\ F_2(K_1,K_2) \\ F_3(K_1,K_2) \\ F_4(K_1,K_2) \end{vmatrix} = R \begin{vmatrix} \Phi_1(K_1,K_2) \\ \Phi_2(K_1,K_2) \\ \Psi_1(K_1,K_2) \\ \Psi_2(K_1,K_2) \end{vmatrix} \qquad (9)$$

The elements of the matrix R are:

$$R_{11} = e^{irz}$$

$$R_{12} = e^{-irz}$$

$$R_{13} = is\, e^{isz}$$

$$R_{14} = -is\, e^{-isz}$$

$$R_{21} = ir\, e^{irz}$$

$$R_{22} = -ir\, e^{-irz}$$

$$R_{23} = e^{isz}(K_\beta^2 - S^2)$$

$$R_{24} = e^{-isz}(K_\beta^2 - S^2)$$

$$R_{31} = 2\mu ir\, e^{irz}$$

$$R_{32} = -2\mu ir\, e^{-irz}$$

$$R_{33} = \mu e^{isz}(K_\beta^2 - 2S^2)$$

$$R_{34} = \mu e^{-isz}(K_\beta^2 - 2S^2)$$

$$R_{41} = -e^{irz}(\lambda K_\alpha^2 + 2\mu r^2)$$

$$R_{42} = -e^{-irz}(\lambda K_\alpha^2 + 2\mu r^2)$$

$$R_{43} = 2\mu e^{isz}\, is\,(K_\beta^2 - S^2)$$

$$R_{44} = -2\mu e^{-isz}\, is\,(K_\beta^2 - S^2)$$

Now consider the m^{th} layer. It's upper surface is $(m-1)^{th}$ interface. Placing the origin of the coordinate system at the $(m-1)^{th}$ interface, using eq. (9), one can write

$$\begin{vmatrix} F_1^{(m-1)}(K_1,K_2) \\ F_2^{(m-1)}(K_1,K_2) \\ F_3^{(m-1)}(K_1,K_2) \\ F_4^{(m-1)}(K_1,K_2) \end{vmatrix} = B_m \begin{vmatrix} \Phi_1^m(K_1,K_2) \\ \Phi_2^m(K_1,K_2) \\ \Psi_1^m(K_1,K_2) \\ \Psi_2^m(K_1,K_2) \end{vmatrix} \qquad (10)$$

where the elements of the matrix B are:

$$B_{ij} = R_{ij}\Big|_{z=0} \qquad \begin{matrix} i = 1, 2, \cdots 4 \\ j = 1, 2, \cdots 4 \end{matrix} \qquad (11)$$

Let the thickness of the m^{th} layer be d_m. Then using eq. (9), one can write

$$\begin{vmatrix} F_1^m(K_1K_2) \\ F_2^m(K_1K_2) \\ F_3^m(K_1K_2) \\ F_4^m(K_1K_2) \end{vmatrix} = A_m \begin{vmatrix} \Phi_1^m(K_1K_2) \\ \Phi_2^m(K_1K_2) \\ \Psi_1^m(K_1K_2) \\ \Psi_2^m(K_1K_2) \end{vmatrix} \qquad (12)$$

where the elements of the matrix A are

$$A_{ij} = R_{ij}\Big|_{z=d_m} \qquad \begin{matrix} i = 1, 2, \cdots 4 \\ j = 1, 2, \cdots 4 \end{matrix}$$

From eqs. (10) and (12)

$$\begin{vmatrix} F_1^{m-1} \\ F_2^{m-1} \\ F_3^{m-1} \\ F_4^{m-1} \end{vmatrix} = B_m A_m^{-1} \begin{vmatrix} F_1^m \\ F_2^m \\ F_3^m \\ F_4^m \end{vmatrix} \qquad (13)$$

$$\begin{vmatrix} F_1^m \\ F_2^m \\ F_3^m \\ F_4^m \end{vmatrix} = A_m B_m^{-1} \begin{vmatrix} F_1^{m-1} \\ F_2^{m-1} \\ F_3^{m-1} \\ F_4^{m-1} \end{vmatrix} \qquad (14)$$

From eq. (10)(*)

$$\begin{vmatrix} \Phi_1^n \\ 0 \\ \Psi_1^n \\ 0 \end{vmatrix} = B_m^{-1} \begin{vmatrix} F_1^{n-1} \\ F_2^{n-1} \\ F_3^{n-1} \\ F_4^{n-1} \end{vmatrix} \qquad (15)$$

Using eq. (14), we have

$$\begin{vmatrix} F_1^{n-1} \\ F_2^{n-1} \\ F_3^{n-1} \\ F_4^{n-1} \end{vmatrix} = A_{n-1} B_{n-1}^{-1} A_{n-2} B_{n-2}^{-1} \cdots A_{s+1} B_{s+1}^{-1} \begin{vmatrix} F_1^{s+} \\ F_2^{s+} \\ F_3^{s+} \\ F_4^{s+} \end{vmatrix} \qquad (16)$$

Therefore,

$$\begin{vmatrix} \Phi_1^n \\ 0 \\ \Psi_1^n \\ 0 \end{vmatrix} = B_m^{-1} A_{m-1} B_{m-1}^{-1} A_{m-2} B_{m-2}^{-1} \cdots A_{s+1} B_{s+1}^{-1} \begin{vmatrix} F_1^{s+} \\ F_2^{s+} \\ F_3^{s+} \\ F_4^{s+} \end{vmatrix} \qquad (17)$$

Let the 4×4 matrix $B_n^{-1} A_{n-1} B_{n-1}^{-1} A_{n-2} B_{n-2}^{-1} \cdots A_{s+1} B_{s+1}^{-1}$ be denoted as the matrix P.

Using eq. (13), one obtains

$$\begin{vmatrix} F_1^{\circ} \\ F_2^{\circ} \\ 0 \\ 0 \end{vmatrix} = B_1 A_1^{-1} \cdots B_s A_s^{-1} \begin{vmatrix} F_1^{s-} \\ F_2^{s-} \\ F_3^{s-} \\ F_4^{s-} \end{vmatrix} \qquad (18)$$

---

* Since there are no source in the half-space, $\Phi_2^n = \Psi_2^n = 0$; (Φ_2^n, Ψ_2^n represent amplitude of plane P and SV waves respectively which travel upward in the half-space).

where F_1^o, F_2^o, etc., refers $F_1(K_1K_2)$ on the 0^{th} interface, i.e. on the free surface.

We consider that at the source level the displacements are continuous but the stresses are not. Let $\Delta p_{ZZ}(x,y)$ be the discontinuity in the normal stress and let the discontinuity in tangential stress $p_{Zx}(x,y)$ be $\frac{\partial}{\partial x}(h(x,y))$ and that in the tangential stress $p_{Zy}(x,y)$ be $\frac{\partial}{\partial y}(h(x,y))$. Let $H_3(K_1K_2)$ and $H_4(K_1K_2)$ be the two-dimensional Fourier transform of $h(x,y)$ and $\Delta p_{ZZ}(x,y)$ respectively. Then

$$\begin{vmatrix} F_1^{S-} \\ F_2^{S-} \\ F_3^{S-} \\ F_4^{S-} \end{vmatrix} = \begin{vmatrix} F_1^{S+} \\ F_2^{S+} \\ F_3^{S+} \\ F_4^{S+} \end{vmatrix} + \begin{vmatrix} 0 \\ 0 \\ H_3 \\ H_4 \end{vmatrix}$$

Therefore, using eq. (18), one obtains

$$\begin{vmatrix} F_1^o \\ F_2^o \\ 0 \\ 0 \end{vmatrix} = B_1 A_1^{-1} \cdots\cdots B_S A_S^{-1} \left\{ \begin{vmatrix} F_1^{S+} \\ F_2^{S+} \\ F_3^{S+} \\ F_4^{S+} \end{vmatrix} + \begin{vmatrix} 0 \\ 0 \\ H_3 \\ H_4 \end{vmatrix} \right\} \qquad (19)$$

Let the matrix product $B_1A_1^{-1}$ .... $B_sA_s^{-1}$ be denoted as the matrix Q.

Using eqs. (17) and (19), one obtains

Note: S^{th} interface is S^+ on the downward side and S^- on the upward side.

$$c) \quad \begin{vmatrix} P_{21} & P_{22} & P_{23} & P_{24} \\ P_{41} & P_{42} & P_{43} & P_{44} \\ Q_{31} & Q_{32} & Q_{33} & Q_{34} \\ Q_{41} & Q_{42} & Q_{43} & Q_{44} \end{vmatrix} \begin{vmatrix} F_1^{s+} \\ F_2^{s+} \\ F_3^{s+} \\ F_4^{s+} \end{vmatrix} = \begin{vmatrix} 0 \\ 0 \\ -(Q_{33} H_3 + Q_{34} H_4) \\ -(Q_{43} H_3 + Q_{44} H_4) \end{vmatrix}$$

Solving eq. (20) for the four unknowns F_1^{s+}, F_2^{s+}, F_3^{s+}, F_4^{s+} one can obtain from eq. (17)

$$\Phi_1^n = P_{11} F_1^{s+} + P_{12} F_2^{s+} + P_{13} F_3^{s+} + P_{14} F_4^{s+}$$

$$\Psi_1^n = P_{31} F_1^{s+} + P_{32} F_2^{s+} + P_{33} F_3^{s+} + P_{34} F_4^{s+} \qquad (20a)$$

$\Phi_1^n (K_1 K_2)$ and $\Psi_1^n (K_1 K_2)$ are the amplitude of P and SV waves respectively in the half-space.

SH Waves.

Displacements and stresses are given by

$$u = \frac{\partial}{\partial y} f_5 (x, y, z)$$

$$v = -\frac{\partial}{\partial x} f_5 (x, y, z) \qquad (21)$$

$$p_{zx} = \mu \frac{\partial}{\partial y} f_6 (x, y, z)$$

$$p_{zy} = -\mu \frac{\partial}{\partial x} f_6 (x, y, z)$$

Functions f_5 (x,y,z), f_6 (x,y,z) are given following eq. (3). Solution of wave eq. (2) is

$$\Lambda(x,y,z) = \frac{1}{2\pi} e^{-i\omega t} \iint_{-\infty}^{+\infty} \left[\Delta_1(k_1,k_2)\, e^{isz} + \Delta_2(k_1,k_2)\, e^{-isz} \right] e^{-i(k_1 x + k_2 y)}\, dk_1\, dk_2 \tag{2.1}$$

where $s^2 + k_1^2 + k_2^2 = \omega^2/\beta^2 = k_\beta^2$

Using eq. (22), functions $f_5(x,y,z)$, $f_6(x,y,z)$ can be written as

$$f_5(x,y,z) = \frac{1}{2\pi} \iint_{-\infty}^{+\infty} \left[\Delta_1(k_1,k_2)\, e^{isz} + \Delta_2(k_1,k_2)\, e^{-isz} \right] e^{+i(k_1 x + k_2 y)}\, dk_1\, dk_2$$

$$f_6(x,y,z) = \frac{1}{2\pi} \iint_{-\infty}^{+\infty} \left[is\,\Delta_1(k_1,k_2)\, e^{isz} - is\,\Delta_2(k_1,k_2) e^{-isz} \right] e^{+i(k_1 x + k_2 y)}\, dk_1\, dk_2 \tag{2.2}$$

On the surface Z = constant, $f_5(x,y,z)\big|_{Z = \text{const.}}$ and $f_6(x,y,z)\big|_{Z = \text{const.}}$ can be written as two-dimensional Fourier integral expansion as follows:

$$f_5(x,y,z)\big|_{z = \text{constant}} = \frac{1}{2\pi} \iint_{-\infty}^{+\infty} F_5(k_1,k_2)\, e^{+i(k_1 x + k_2 y)}\, dk_1\, dk_2$$

$$f_6(x,y,z)\big|_{z = \text{constant}} = \frac{1}{2\pi} \iint_{-\infty}^{+\infty} F_6(k_1,k_2)\, e^{+i(k_1 x + k_2 y)}\, dk_1\, dk_2 \tag{2.4}$$

From eqs. (23) and (24) one can write

$$\begin{vmatrix} e^{isz} & e^{-isz} \\ is\,e^{isz} & -is\,e^{-isz} \end{vmatrix} \begin{vmatrix} \Delta_1 \\ \Delta_2 \end{vmatrix} = \begin{vmatrix} F_5(k_1,k_2) \\ F_6(k_1,k_2) \end{vmatrix} \tag{2.5}$$

Let the 2 x 2 matrix on the left-hand side of eq. (25) be

denoted as L. All the elements of the matrix L are to be evaluated at Z = constant.

Now consider the m^{th} layer again. Placing the origin of the coordinate at $(m-1)^{th}$ interface, using eq. (25), one obtains

$$\begin{vmatrix} F_5^{(m-1)}(K_1K_2) \\ F_6^{(m-1)}(K_1K_2) \end{vmatrix} = D_m \begin{vmatrix} \Delta_1^m(K_1K_2) \\ \Delta_2^m(K_1K_2) \end{vmatrix} \qquad (26)$$

where the elements of the matrix D are:

$$D_{ij} = L_{ij}\Big|_{Z=0} \qquad \begin{matrix} i = 1,2 \\ j = 1,2 \end{matrix}$$

Let the thickness of the m^{th} layer be d_m. Then, using eq. (25) one obtains

$$\begin{vmatrix} F_5^m(K_1K_2) \\ F_6^m(K_1K_2) \end{vmatrix} = C_m \begin{vmatrix} \Delta_1^m(K_1K_2) \\ \Delta_2^m(K_1K_2) \end{vmatrix} \qquad (27)$$

where the elements of the matrix C are

$$C_{ij} = L_{ij}\Big|_{Z=d_m} \qquad \begin{matrix} i = 1,2 \\ j = 1,2 \end{matrix}$$

From eqs. (26) and (27), one can write

$$\begin{vmatrix} F_5^{(m-1)} \\ F_6^{(m-1)} \end{vmatrix} = D_m C_m^{-1} \begin{vmatrix} F_5^m \\ F_6^m \end{vmatrix} \qquad (28)$$

and

and

$$\begin{vmatrix} F_5^m \\ F_6^m \end{vmatrix} = C_m D_m^{-1} \begin{vmatrix} F_5^{m-1} \\ F_6^{m-1} \end{vmatrix} \qquad (29)$$

From eq. (26), one obtains

$$\begin{vmatrix} \Delta_1^m (K_1 K_2) \\ C \end{vmatrix} = D_m^{-1} \begin{vmatrix} F_5^{n-1} (K_1 K_2) \\ F_6^{n-1} (K_1 K_2) \end{vmatrix} \qquad (30)$$

Using eq. (29), one obtains

$$\begin{vmatrix} F_5^{n-1} \\ F_6^{n-1} \end{vmatrix} = C_{n-1} D_{n-1}^{-1} \cdots C_{s+1} D_{s+1}^{-1} \begin{vmatrix} F_5^{s+} \\ F_6^{s+} \end{vmatrix}$$

There fore,

$$\begin{vmatrix} \Delta_1^m \\ 0 \end{vmatrix} = D_m^{-1} C_{m-1} D_{m-1}^{-1} C_{m-2} D_{m-2}^{-1} \cdots C_{s+1} D_{s+1}^{-1} \begin{vmatrix} F_5^{s+} \\ F_6^{s+} \end{vmatrix} \qquad (31)$$

Let the matrix product $D_n^{-1} C_{n-1} D_{n-1}^{-1} \cdots C_{s+1} D_{s+1}^{-1}$ be denoted as the matrix X.

Using eq. (28), one obtains

$$\begin{vmatrix} F_5^0 \\ C \end{vmatrix} = D_1 C_1^{-1} \begin{vmatrix} F_5^1 \\ F_6^1 \end{vmatrix} = D_1 C_1^{-1} D_2 C_2^{-1} \cdots D_s C_s^{-1} \begin{vmatrix} F_5^{s-} \\ F_6^{s-} \end{vmatrix}$$

Again we assume

$$\begin{vmatrix} F_5^{s-} \\ F_6^{s-} \end{vmatrix} = \begin{vmatrix} F_5^{s+} \\ F_6^{s+} \end{vmatrix} + \begin{vmatrix} 0 \\ H_6 \end{vmatrix}$$

then

$$\begin{vmatrix} F_5^{0} \\ 0 \end{vmatrix} = D_1 C_1^{-1} D_2 C_2^{-1} \cdots D_5 C_5^{-1} \left\{ \begin{vmatrix} F_5^{s+} \\ F_6^{s+} \end{vmatrix} + \begin{vmatrix} 0 \\ H_6 \end{vmatrix} \right\} \tag{32}$$

Let us denote the matrix product

$$D_1 C_1^{-1} D_2 C_2^{-1} \cdots D_5 C_5^{-1} \text{ as } Y$$

From eqs.(31) and (32) one obtains

$$\begin{vmatrix} X_{21} & X_{22} \\ Y_{21} & Y_{22} \end{vmatrix} \begin{vmatrix} F_5^{s+} \\ F_6^{s+} \end{vmatrix} = \begin{vmatrix} 0 \\ -Y_{22} H_6 \end{vmatrix} \tag{33}$$

Solving for two unknowns F_5^{s+}, F_6^{s+}, one obtains using eq.(31)

$$\Delta_1^{n} = X_{11} F_5^{s+} + X_{12} F_6^{s+} \tag{33a}$$

which is the amplitude of plane SH waves in the half-space.

Two-dimensional Fourier transform of different kinds stress distributions

$H(K_1K_2)$ functions for P and SV waves.

(1) a single vertical force acting at the origin in the positive Z-direction:

$$p_{zz}(x,y) = F_z\,\delta(x)\,\delta(y)$$

$$p_{zx}(x,y) = p_{zy}(x,y) = 0$$

$$H(k_1,k_2) = \frac{F_z}{2\pi}$$

(2) a single vertical couple with counterclockwise moment about an axis in the x-y plane, making angle φ with the x-axis - the moment arm is 2ϵ.

$$M_H = \lim_{\epsilon \to 0} F_z \cdot 2\epsilon$$

$$p_{zx} = p_{zy} = 0$$

$$p_{zz}(x,y) = -F_z\,\delta(x - \epsilon\cos\varphi)\,\delta(y - c\sin\varphi) + F_z\,\delta(x + \epsilon\cos\varphi)\,\delta(y + \epsilon\sin\varphi)$$

$$H(k_1,k_2) = \frac{M_H}{2\pi}\, i\,(k_1\cos\varphi + k_2\sin\varphi)$$

(3a) two couples with opposing senses in the x-y plane. The moment arm, 2ϵ, makes an angle φ with the X-axis

$$M_{zx} = \lim_{\epsilon \to 0} F_x \cdot (2\epsilon \sin\varphi)$$

$$M_{zy} = \lim_{\epsilon \to 0} F_y \cdot (2\epsilon \sin\varphi)$$

$$p_{zx}(x,y) = \mu \frac{\partial}{\partial x} f_3(x,y) + \mu \frac{\partial^2 \Lambda}{\partial z \partial y}$$

$$p_{zy}(x,y) = \mu \frac{\partial}{\partial y} f_3(x,y) - \mu \frac{\partial^2 \Lambda}{\partial z \partial x}$$

$$\frac{\partial}{\partial x}(p_{zx}) + \frac{\partial}{\partial y}(p_{zy}) = \mu \left\{ \frac{\partial^2}{\partial x^2}\left[f_3(x,y)\right] + \frac{\partial^2}{\partial y^2}\left[f_3(x,y)\right] \right\}$$

taking Fourier transform of both sides, one obtains

$$-\mu(k_1^2 + k_2^2) H(k_1,k_2) = i k_1 \left[\bar{P}_{zx}\right] + i k_2 \left[\bar{P}_{zy}\right]$$

where

$\bar{P}_{zx}$, $\bar{P}_{zy}$ are the Fourier transform of $p_{zx}(x,y)$ and $p_{zy}(x,y)$ respectively. It turns out that

$$H(k_1,k_2) = \frac{1}{2\pi\mu(k_1^2+k_2^2)} \left[k_2 M_{zy}(k_1 + k_2 \tan\varphi) - k_1 M_{zx}(k_1 \cot\varphi + k_2)\right]$$

$$\varphi \neq n\pi, \qquad n = 0, 1$$
$$\varphi \neq (2n+1)\frac{\pi}{2}$$

The above system reduces to a single couple if either

$M_{zx} >> M_{zy}$ or $M_{zy} >> M_{zx}$. In that case in the

expression for $H(K_1K_2)$ above one can neglect either M_{Zx} or M_{Zy}. In case $M_{zy} = -M_{zx} = M$, then

$$H(k_1k_2) = \frac{M}{2\pi\mu(k_1^2+k_2^2)}\left[2k_1k_2 + k_2^2\tan\varphi + k_1^2\cot\varphi\right]$$

$$\varphi \neq n\pi$$
$$\varphi \neq \left(\frac{2n+1}{2}\right)\pi \qquad n = 0, 1$$

(3b) horizontal double couple

$$M_{zx} = \lim_{\epsilon\to 0} Fx.(2\epsilon)$$

$$M_{zy} = \lim_{\epsilon\to 0} Fy.(2\epsilon)$$

$$p_{zx} = \mu\frac{\partial}{\partial x} f_3(x,y) + \mu\frac{\partial^2 V}{\partial z\,\partial y}$$

$$p_{zy} = \mu\frac{\partial}{\partial y} f_3(x,y) - \mu\frac{\partial^2 V}{\partial z\,\partial x}$$

$$\frac{\partial}{\partial y}(p_{zx}) + \frac{\partial}{\partial y}(p_{zy}) = \mu\left(\frac{\partial^2}{\partial x^2} + \frac{\partial^2}{\partial y^2}\right) f_3(x,y)$$

taking two-dimensional Fourier transform of both sides, one obtains

$$-\mu(k_1^2+k_2^2)\,H(k_1k_2) = ik_1\bar{P}_{zx} + ik_2\bar{P}_{zy}$$

where $\bar{P}_{Zx}$ and $\bar{P}_{Zy}$ are Fourier transform of $p_{Zx}(x,y)$ and $p_{Zy}(x,y)$ respectively. It turn out that

$$H(K_1K_2) = -\frac{1}{2\pi\mu}\frac{K_1K_2}{(K_1^2+K_2^2)}(M_{zx}+M_{zy})$$

if $M_{zx} = M_{zy}$, then

$$H(K_1K_2) = -\frac{M}{\pi\mu}\frac{K_1K_2}{(K_1^2+K_2^2)}$$

$H(K_1K_2)$ functions for SH waves.

A pair of horizontal couples.

$$p_{zx}(x,y) = \mu\frac{\partial}{\partial x}f_3(x,y) + \mu\frac{\partial}{\partial y}f_6(x,y)$$

$$p_{zy}(x,y) = \mu\frac{\partial}{\partial y}f_3(x,y) - \mu\frac{\partial}{\partial x}f_6(x,y)$$

Therefore,

$$\frac{\partial}{\partial y}(p_{zx}) - \frac{\partial}{\partial x}(p_{zy}) = \mu\left(\frac{\partial^2}{\partial x^2}+\frac{\partial^2}{\partial y^2}\right)f_6(x,y)$$

taking Fourier transform of both sides, one obtains

$$-\mu(K_1^2+K_2^2)H(K_1K_2) = iK_2\bar{P}_{zx} - iK_1\bar{P}_{zy}$$

$$\bar{P}_{zx} = \frac{-i}{2\pi}M_{zx}(K_1\cot\varphi + K_2)$$

$$\bar{P}_{zy} = \frac{iM_{zy}}{2\pi}(K_1 + K_2\tan\varphi)$$

$$H(K_1K_2) = -\frac{1}{2\pi\mu(K_1^2+K_2^2)}\left[M_{zx}K_2(K_1\cot\varphi + K_2) + M_{zy}K_1(K_1 + K_2\tan\varphi)\right]$$

Discussion

A system of forces of harmonic time variation having arbitrary orientation acts on the S^{th} interface. The amplitude of plane P, SV and SH waves which propagate along a direction

in the half-space are expressed in terms of the two-dimensional spatial Fourier transform $H(K_1K_2)$ of force distribution on the source level. Two-dimensional Fourier transform $H(K_1,H_2)$ is calculated for different kinds of stress distribution. If these $H(K_1K_2)$ functions are used in eq. (20) (in the case of P and SV waves) and in eq. (33) (in the case of SH waves), one would obtain by using eqs. (20a) and (33a) the amplitude of P, SV and SH waves which propagate along a particular direction in the half-space.

At the present time computer programs are being written for various phases of computational work. The object of computation is to calculate Φ_1^n, Ψ_1^n, Λ_1^n for different ω for various distributions of forces at the source level and various depths of the source interface.

Reference

Harkrider, D.G., 1964, "Surface waves in multilayered elastic media: I. Rayleigh and Love waves from buried sources in a multilayered elastic half-space," Bull. Seism. Soc. Am., 54, pp. 627-679.

6. Model Studies

Analogue Spectral Techniques

The research in seismic model techniques originated during the period of this report was devoted primarily to the development of rapid analogue techniques for extracting spectral information from the signals generated in the model system. In previous model investigations of wave generation and propagation, using primarily explosive sources, but also pulsed ceramic transducers, analysis was done in the time domain or in the frequency domain, using digital methods to extract the spectrums.

The acquisition of two new items of laboratory instrumentation by the Department has made possible this development of the capability of the seismic models laboratory. One item, suitable for on-line examination of the main spectral characteristics of the signal produced by a repetitively-pulsed source, is a Nelson-Ross Model 013 spectrum analyzer. The other is a Kay Electric Company Model 7029A Sound Spectrograph.

The Nelson-Ross analyzer plugs into a Tektronix 535A Oscilloscope. It can be used to display the entire spectrum of a repetitive signal from 0 to 500 kHz, or any desired frequency can be selected as a center frequency of the display and by means of a dispersion control a detailed presentation of any portion of the spectrum can be obtained. An auxiliary function generator is used as a control on the calibration. The analyzer requires a repeated signal, and so far has only been applied to pulsed transducers and continuous wave inputs. The system can be applied to explosion signals by recording on magnetic tape and forming a tape loop.

A disadvantage of the present method of application is that the entire signal, including all body and surface waves, is processed. It is planned to incorporate a gating circuit that will pass only a preselected portion of the signal, e.g., the first arriving P-wave.

The first application of the Kay Sound Spectrograph to the analysis of seismic transients was reported by Ewing, et al. (1959) and Landisman, et al. (1962). In their work it was necessary to speed up the playback of the data in order to put the signal into the range of the spectrograph. In model seismology the problem is the reverse: the energy is mostly in the range of tens of kilo-Hertz, so that a slowed-down replay is required. This has been achieved by recording the signals on a Precision Instrument Model PS-207A Instrumentation Recorder at 60 ips, direct record, and playing back at 1 7/8 ips. Frequencies are divided by 32, putting the signal into the 0-16 kHz range of the spectrograph. The chief limitation is the 100 kHz high frequency cut-off of the tape recorder.

The two displays available from the spectrograph that are most useful for this work are illustrated in Figures 11 and 12. Figure 11 illustrates the Sonogram, a frequency-amplitude-time display. The horizontal axis is time, the vertical axis is frequency increasing upward, and the amplitude is shown by relative darkness. Frequencies indicated next to the calibration marks have been converted to real frequencies and the time scale corresponds to original real time. The arrival of the transient from the explosion in Plexiglas is clearly seen, followed by low frequency reverberations. Although the time scale is very

SONAGRAM

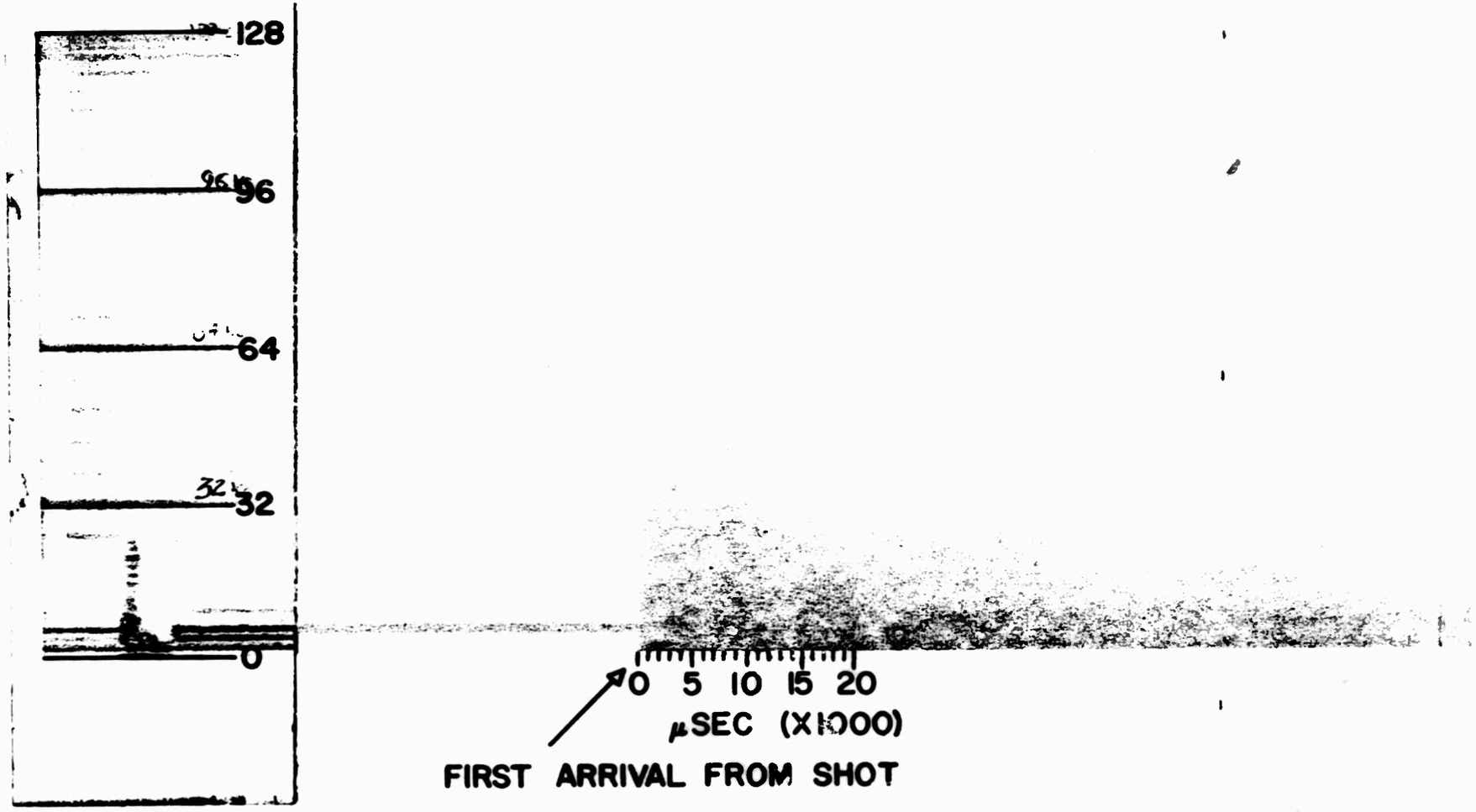

FIG· 11

SONAGRAM SECTIONS

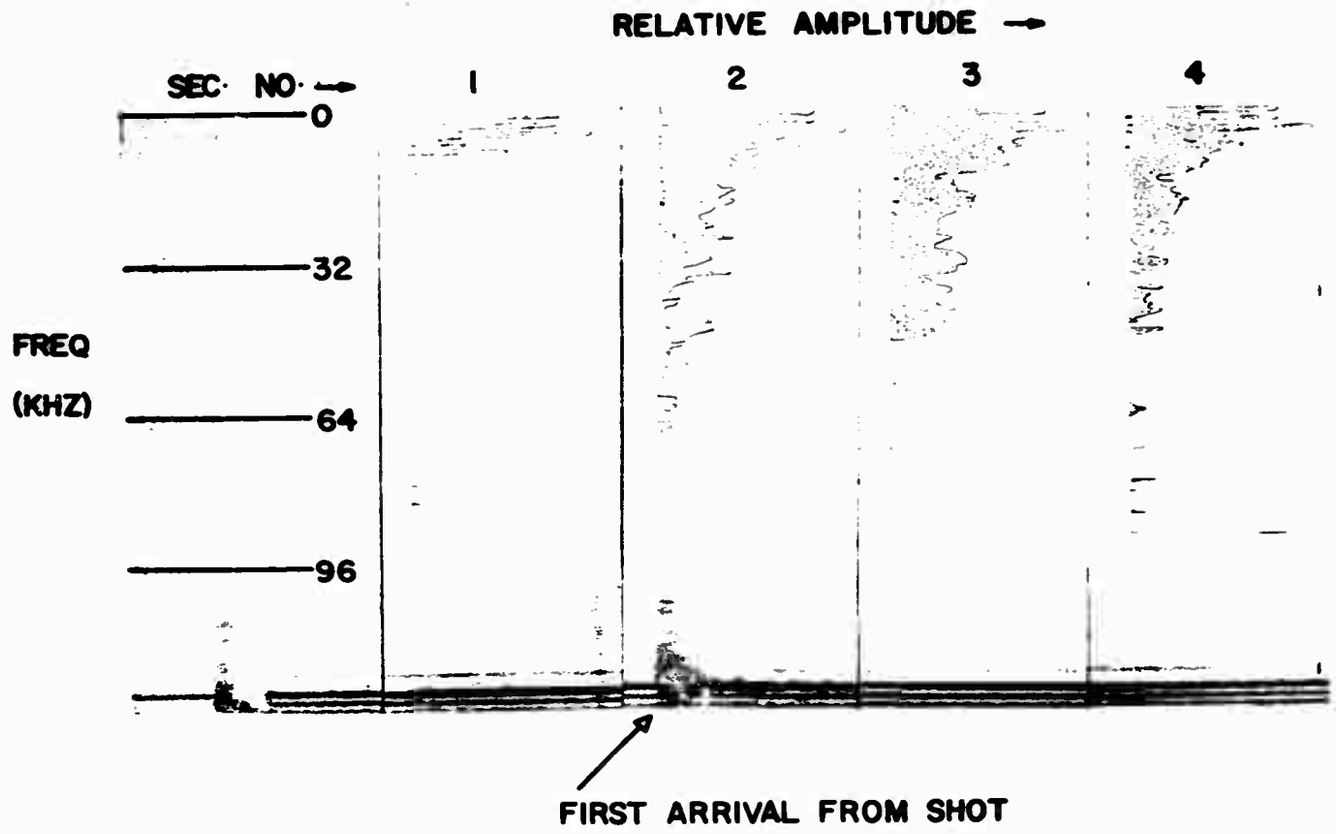

FIG. 12

compressed, a detailed interpretation is possible by the technique discussed next.

The displays in Figure 12 are called sections. A section can be taken at any preselected point in the signal. Amplitude versus frequency (increasing downward) is shown at the times selected. By moving through the signal in small increments of time, a complete picture of the growth of the spectrum as time passes can be assembled. The analysis of the data in Figure 12 is discussed below.

A variety of tests were made to determine the effects on the signal of processing through several instruments. The output of the detectors as developed on an oscilloscope was photographed and used as the"true"record for comparison purposes. The signal as recorded both in the tape recorder and in the tape loop of the spectrograph was played into a Brush oscillograph. It was clear that, in the lower frequencies at least, little is lost in going from the recorder to the spectrograph. The tape recorder itself gives a faithful reproduction when played back at the slow speed. This test was of limited value because the Brush oscillograph itself did not pass signals above 2.5 kHz, so that the fidelity at the higher frequencies could not be tested.

A measure of the reproducibility may be seen in the seismograms in Figure 13. The records for 13a and b are from two different shots in Plexiglas. In 13c, the signal that produced 13b has been put through the magnetic tape recorder and played back at 1/32 of the signal speed. The time scale on the oscilloscope has been adjusted accordingly. Unfortunately, because of triggering problems, the onset, the most interesting part, is not seen

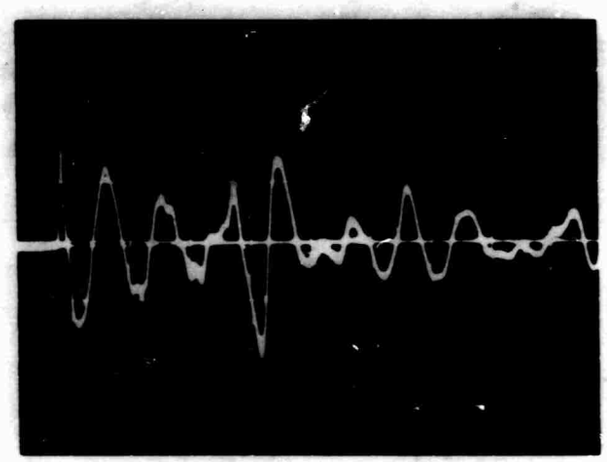

(A)

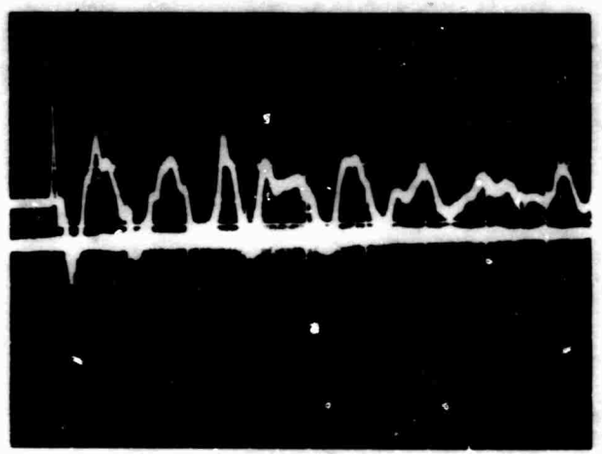

(B)

FIG. 13

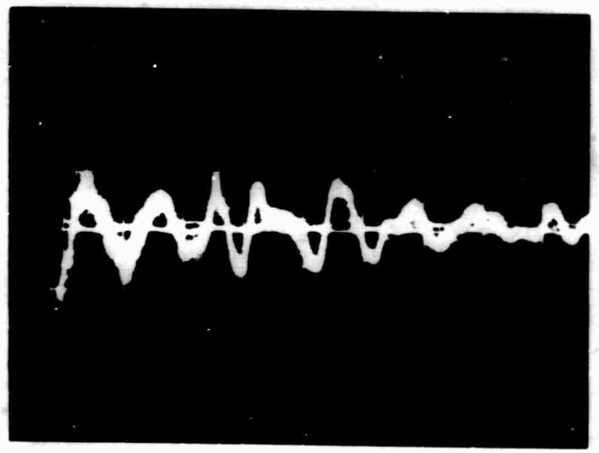

(C)

in 13c, but the rest of the record shows that the signal is faithfully reproduced in the slow-down procedure.

A thorough calibration of the spectrograph was conducted, using continuous sine waves and square wave pulses. Both the frequency calibration and the time calibration along the record were checked.

As an independent test, the overall frequency response of the entire system, source through medium and receiver, was determined by driving the source with a sinusoidal voltage with variable frequency. Peaks in the output were noted and compared with those determined by the two spectrum analyzers. The most important finding of this series of experiments was that most of the spectral peaks were associated with sharp resonances in the driving and receiving transducers. Various mountings and transducer holders were tried, but some strong resonances still occurred within the part of the spectrum in which the pulse employed for generating transients had most of its energy. In addition, the spectrum proved sensitive to the pressure with which the crystal was held against the medium. For those reasons explosive sources and capacitance transducers were used in subsequent studies. This source and receiver system has been proven through many years of work in this laboratory. The contrast in the signals produced by crystal and capacitance detectors may be seen in Figures 14a and 14b, respectively. The source is an explosion in Plexiglas. The capacitor transducers are less sensitive than the ceramic ones, so that the voltage from the function generator was too low to produce a detectable signal.

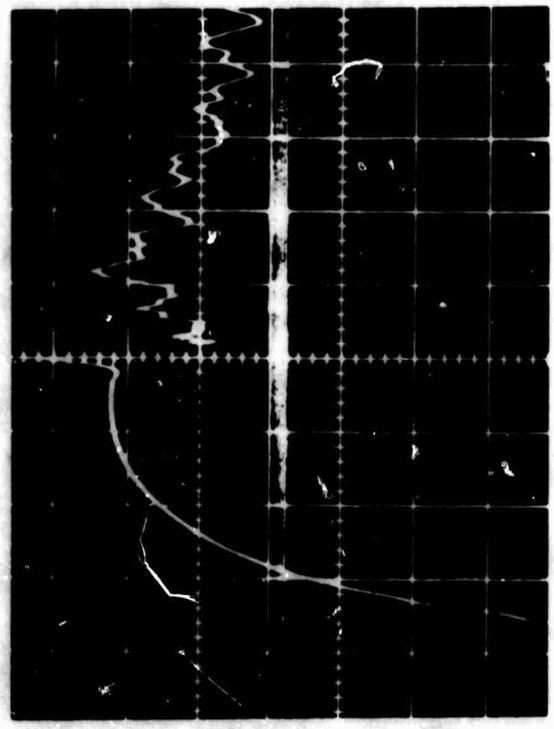

(B)

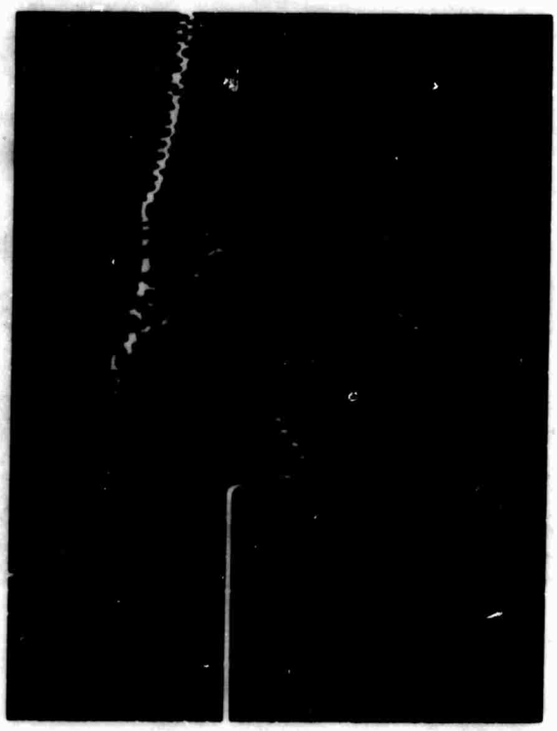

(A)

FIG. 14

Preliminary Experiments.

As a test of the methods of analysis, a series of experiments on the frequency dependence of transmission through a layer over a half-space was conducted. This is a problem receiving much attention in seismology today in an effort to account for the effects of crustal structure on the recorded surface motion. When the effectiveness of the analogue techniques and the experimental methods are firmly established, related problems of greater mathematical difficulty, such as transmission through dipping layers will be attacked.

In the experiments, the source was far enough from the surface (five wavelengths or more) that plane wave theory was applicable. Only normal incidence at the base of the layer was considered.

In the first series of experiments, aluminum was used as the half-space, with Plexiglas as the layer. First, the spectrums were observed at a point in the interior of the half-space and at the free edge (before the Plexiglas layer was put in place) for a lead titanate-zirconate source driven by both a repeated pulse and a sine wave generator. Then the layer was added and the observations on the top of the layer made.

Because the input signal in aluminum for a pulse source is rich in high frequencies, the magnetic tape recorder was inadequate. Spectrums obtained with the Nelson-Ross analyzer and by observing the response to continuous sine waves are shown in Figures 15 and 16. In both figures ceramic transducers were used as both source and receiver. The source was in the interior of an aluminum sheet. The receiver was at the surface. The

ANALOG PLUG-IN

SPECTRUM ANALYZER

FIG. 15

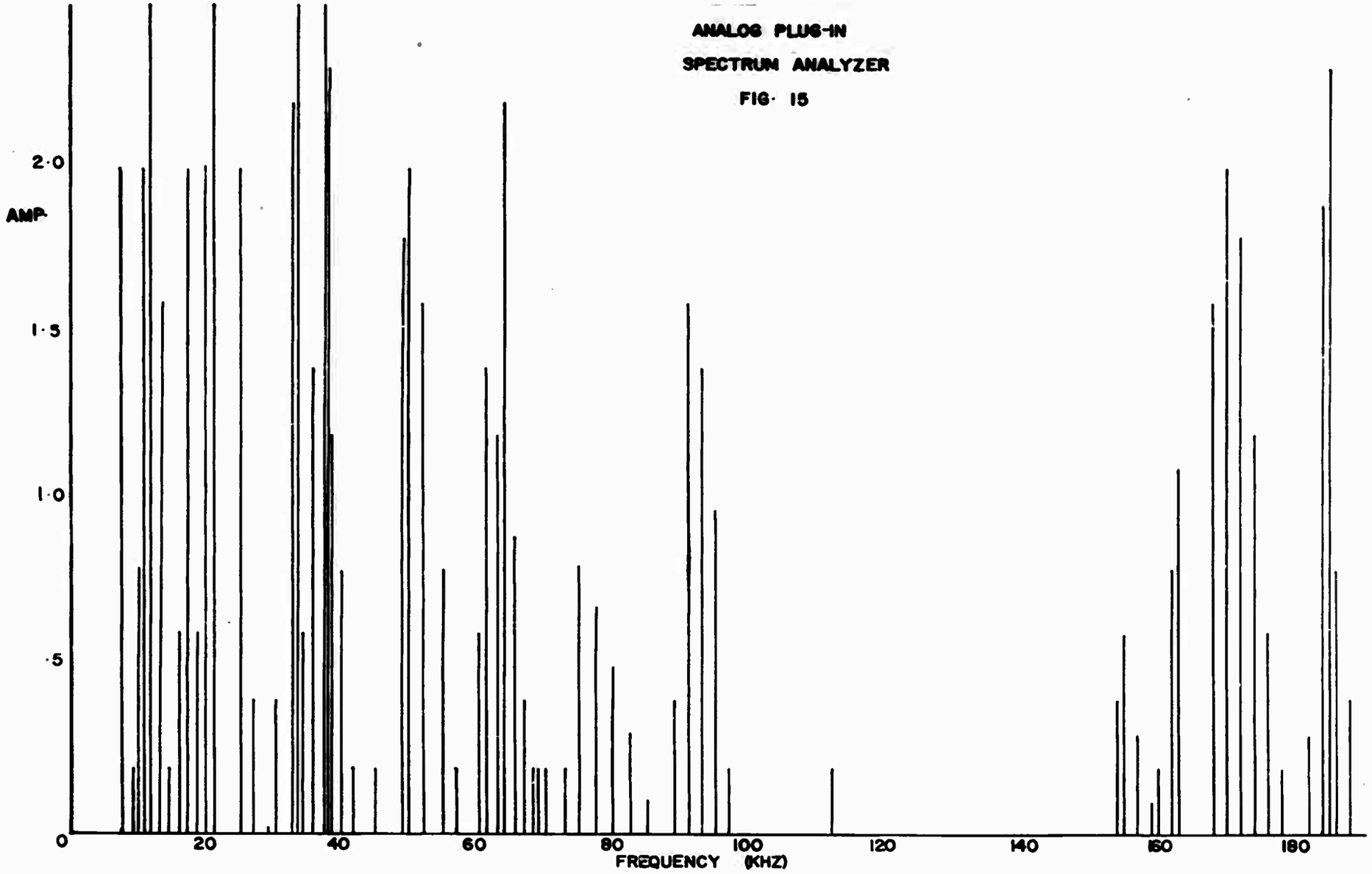

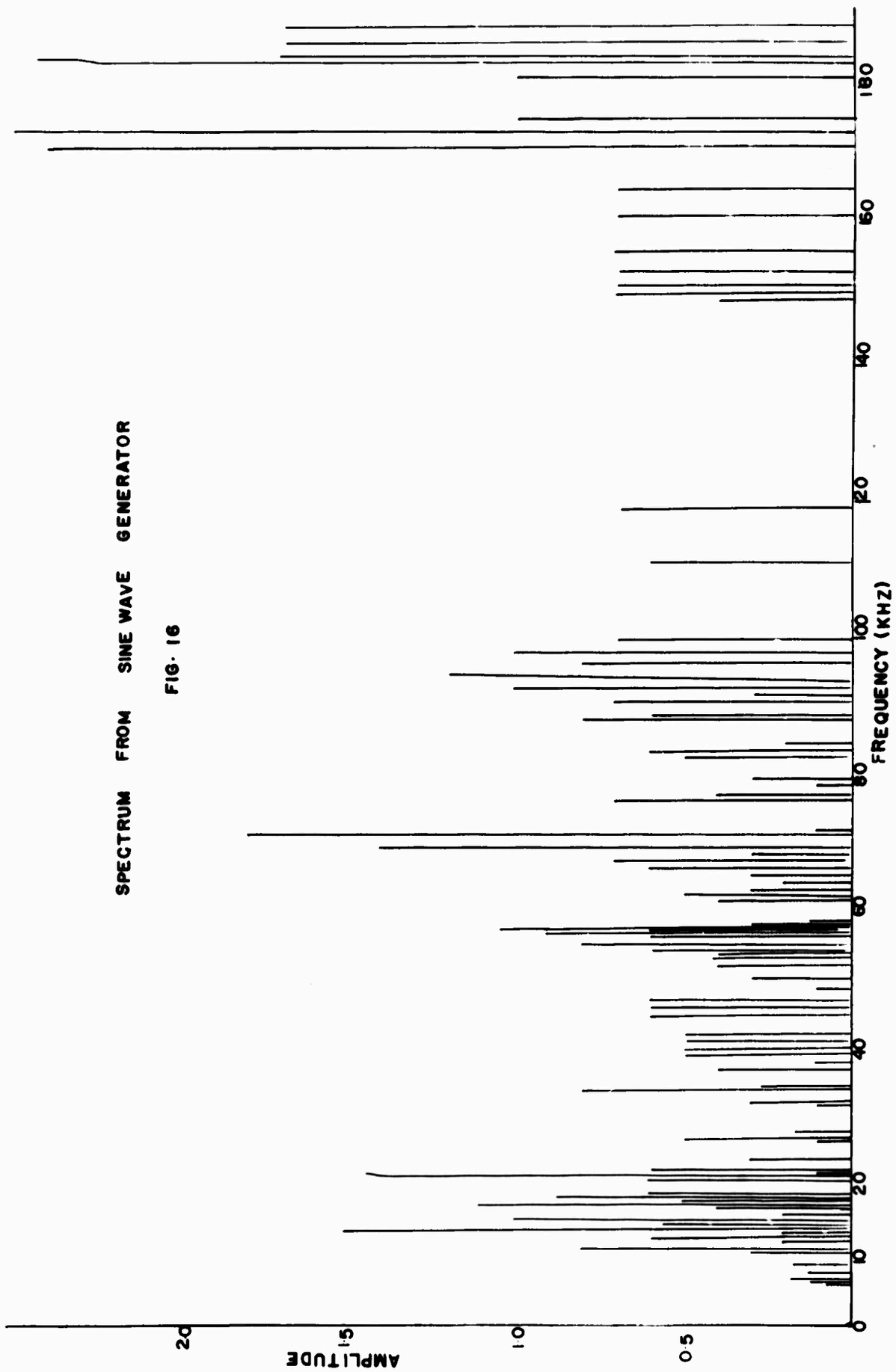

FIG. 16

SPECTRUM FROM SINE WAVE GENERATOR

results show that the analyzer gives a satisfactory picture of the spectrum. The peaks in these figures correspond to resonances in the transducers.

It was known from previous experience that impulsive sources in Plexiglas produced signals with spectrums that peaked at frequencies well within the range of the tape recorder. Therefore, subsequent experiments used Plexiglas as the half-space and Styrofoam as the low-velocity surface layer. It was also anticipated, however, that because of high attenuation in Plexiglas the function generator would not produce detectable signals, especially when capacitor pickups were being used. Therefore, explosions were used as the source.

A layer of Styrofoam 10 cm deep was cemented to a Plexiglas sheet. The pertinent properties, plate velocity and density of the materials are:

	V_p (km/sec)	P (gm/cm^3)
Plexiglas	2.3	1.22
Styrofoam	0.9	0.03

A comparison of the spectrum of the P-wave as derived by stated digital methods and by use of the Kay spectograph is shown in Figure 17. The digital spectrum corresponds to a time from onset to 250 μ sec. The analogue spectrum was derived from the Sonograph sections given in Figure 12. The first section in Figure 12 represents the noise preceding the onset. The next three sections are separated at intervals of 130 μ secs (in real model time), starting as close to the event as the system could be set. The three sections, then, cover the same time window as the digital spectrum. The noise of section 1 was

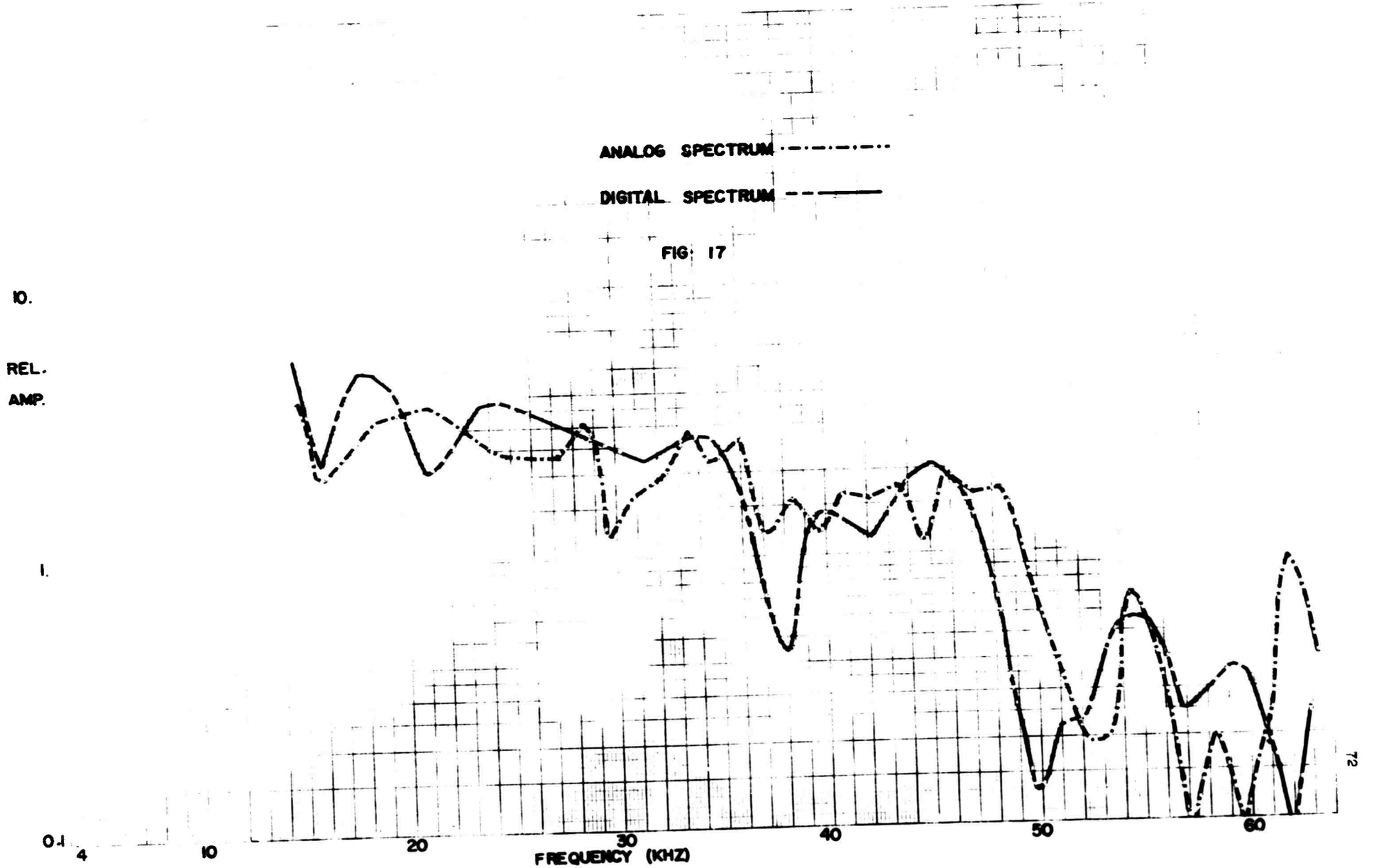
ANALOG SPECTRUM
DIGITAL SPECTRUM
10.
REL.
AMP.
1.
0.1
4
10
20
30
40
50
60
FREQUENCY (KHZ)

FIG. 17

subtracted graphically from the other three. Then the three sections were added to give an equivalent integrated spectrum. The curves shown in Figure 17 demonstrate that the two methods give results which are quite close.

In preparation for the first thorough test of the methods, the transmission coefficient through a single low-velocity layer over a half-space was determined. The spectrum of the wave incident at the base of the layer and that observed at the top were divided to yield the frequency-dependent transmission coefficient:

$$|T(\omega)| = \frac{|O(\omega)|}{|I(\omega)|}$$

where $I(\omega)$ and $O(\omega)$ are the observed input and output spectrums respectively. $I(\omega)$ is the digital curve in Figure 17. The experimental result is shown in Figure 18. Three pronounced peaks occur at 13, 18, and 24 kHz.

Simple theory for the problem studied, e.g. Backus (1959), predicts peaks at 2250, 6750, 11,250, 16,750, etc. A slight change in the plate velocity in the layer, from 0.9 to 1.1 km/sec puts these peaks at 2750, 8250, 13750, 19,250, 24,750, etc. The actual speed in the sample of Styrofoam used will be remeasured to determine if the slight shift of these peaks can be explained this way.

The reason for the lack of transmission peaks above 24 kHz is not clear. The input spectrum contains significant energy out to about 50 kHz, and yet these high frequencies are lost in transmission. Further examination of the absorptive properties of the Styrofoam may clear this up.

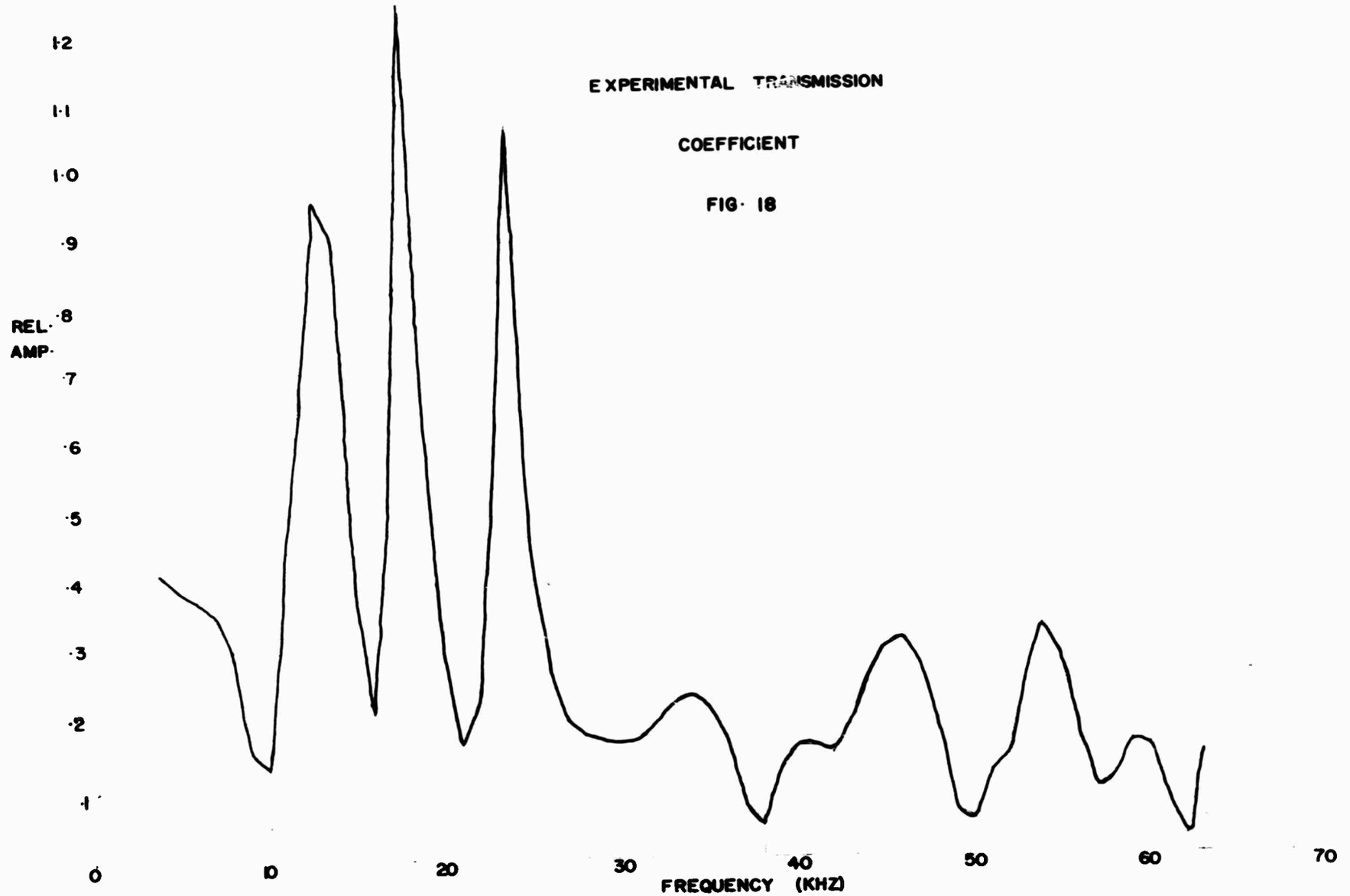
EXPERIMENTAL TRANSMISSION
COEFFICIENT
FIG. 18
REL. AMP.
1·2
1·1
1·0
·9
·8
·7
·6
·5
·4
·3
·2
·1
0
10
20
30
40
50
60
70
FREQUENCY (KHZ)

The next step will be to use strictly analogue techniques to determine the transmission coefficient and compare the results. If they are successful, the dipping bed problem will be attacked.

References

Backus, M.M. (1959), "Water Reverberations - Their Nature and Elimination," Geophysics, 24: 233-261.

Ewing, M., S. Mueller, M. Landisman, and Y. Sato (1959), "Transient Analysis of Earthquake Explosion Arrivals," Geofisica pura e applicata, 44: 83-118.

Landisman, M., S. Mueller, B. Bolt, and M. Ewing (1962), "Transient Analysis of Seismic Core Phases," Geofisica pura e applicata, 52: 41-52.

B. Summaries of Work Completed.

1. "Love and Rayleigh Wave Phase Velocities over U.S. Continental Paths," by Michael L. Goodwin. Summary of Ph.D. dissertation, September, 1968.

Surface waves of nine earthquakes, with propagation paths crossing the United States, were chosen for analysis. The Love and Rayleigh waves were digitized from seismograms of both WWSSN and LRSM stations. The use of both networks of stations provided a greater number of possible profiles in the area approximately bounded by the Rocky Mountains on the west, and the Appalachian Mountains on the east. A total of 94 profiles, shown in Figure 19 were used in this study.

The digitized data,smoothed, detrended and mean removed, were Fourier analyzed in the period range between 10 and 70 seconds, and corrected for instrumental effects. The phase velocities between pairs of stations were computed, using the difference in arrival times of the Fourier components at each of the two stations of the pair. An iteration-least squares inversion process was applied to the observed Love wave and Rayleigh wave phase velocities to obtain the shear velocity distribution down to about 200 km deep. An earth model of 15 layers (for the 200 km depth) was used, allowing more detailed results than have been obtained from thicker layered models. The calculations for the Fourier analysis and phase velocity and the inversion procedures were run on the IBM 360/50 computer at Washington University, St. Louis, Missouri.

The results of the inversions show a crust slightly greater than 40 km in the north-central United States. The crust thickens to nearer 50 km under the southern Canadian Shield, Lake Michigan and the northern Appalachian Mountains. The western edge of the Great Plains area has a crust which is close to 50 km thick, perhaps greater, and which thins toward 40 km in northern New Mexico. In southern Arizona and southern New Mexico the crust is about 40 km thick, as it is in the central United States and Gulf Coast areas.

Except for the Gulf Coast area, most of the profiles indicate a low-velocity channel in the crust and in the mantle. The low-velocity channel in the crust begins at about 21 km and extends to about 26 km depth. The low-velocity channel in the mantle usually lies between 80 and 180 km deep. In the places in which the low-velocity channel is thinner, it often begins between 60 and 80 km deep. See Figures 20 and 21.

In the Gulf Coast area, the evidence for the low-velocity channels in the crust and mantle indicate that

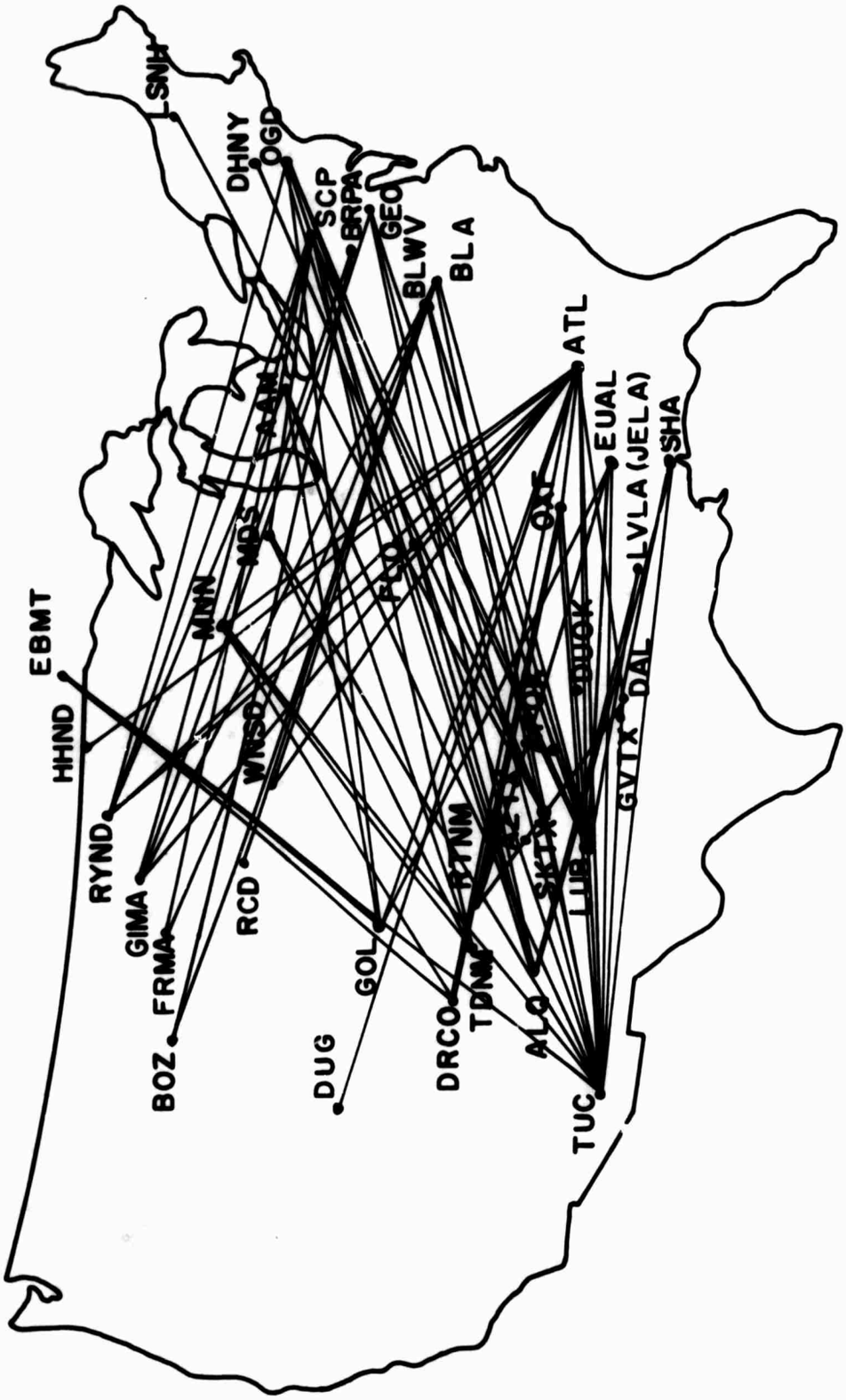

Figure 19. Map of Phase Velocity Profiles.

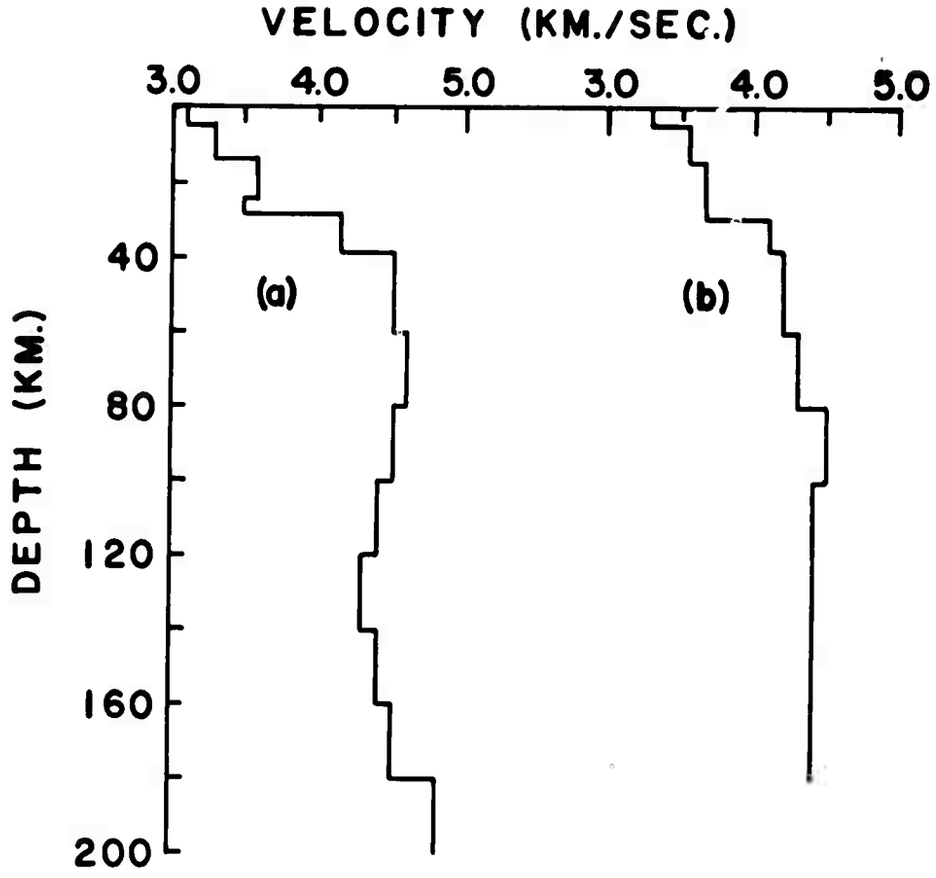

Figure 20. Shear Velocity vs. Depth Profiles for (a) north-central United States and (b) southern Canadian Shield-Great Lake Area.

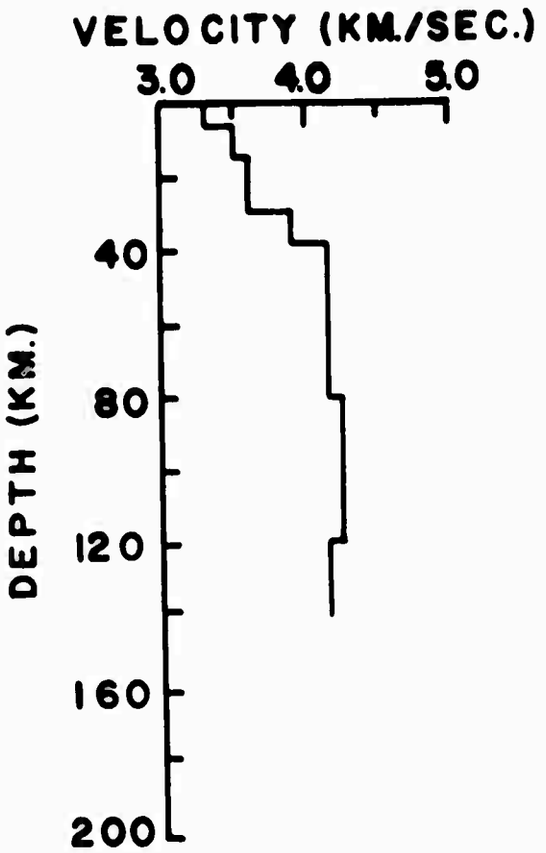

Figure 21. Shear Velocity vs. Depth Profile for the Arizona-New Mexico to north-central United States Area.

the low-velocity channel in the crust disappears, and the low-velocity channel in the mantle either disappears or its depth is beyond the range of the data. These results are summarized in the table.

TABLE

SUMMARY OF SHEAR VELOCITY MODELS.

PROFILE, TABLE NO.		CRUST THICK. (KM)	LVC IN CRUST DEPTH (KM)	LVC IN CRUST VEL. (KM/SEC)	LVC IN MANTLE DEPTH (KM)	LVC IN MANTLE VEL. (KM/SEC)
NORTH-CENTRAL U.S., SOUTHERN CANADIAN SHIELD, GREAT LAKES AREAS.						
ATL-HHND,	8	40	26-40	3.62	120+	4.37
ATL-GIMA,	97	38	26-38	3.56	80+	4.48
ATL-MNN,	9	26	21-26	3.54	60-80	4.40
ATL-WNSD,	95	26	NONE	-	100+	4.52
BLA-BOZ,	92	38	21-26	3.49	100-160	4.28
BLA-WNSD,	94	38	21-26	3.56	*	-
BRPA-BOZ,	77	32	21-26	3.42	60+	4.28
FRMA-BLA,	20	26	NONE	-	80-160	4.30
GIMA-BLA,	23	32	NONE	-	60-140	4.10
GIMA-GEO,	60	32	NONE	-	80+	4.18
SCP-GIMA,	15	26	21-26	3.51	100+	4.41
GIMA-SCP,	57	38	21-26	3.57	100+	4.36
RYND-OGD,	56	26	21-26	3.41	100-160	4.22
BRPA-MNN,	87	50	NONE	-	*	-
ARIZONA-NEW MEXICO TO NORTH-CENTRAL U.S. AREA.						
TDNM-MDS,	41	40	21-26	3.62	60-100	4.11
TDNM-MNN,	49	38	NONE	-	100-120	4.37
TUC-AAM,	44	38	NONE	-	80-160	4.13
TUC-MDS,	51	32	21-26	3.56	100+	4.16
TUC-MNN,	25	38	NONE	-	*	-
TUC-EBMT,	45	40	NONE	-	*	-
DRCO-EBMT,	48	40-50	NONE	-	120+	4.40

TABLE (CONTINUED)

PROFILE, TABLE NO.		CRUST THICK. (KM)	LVC IN CRUST DEPTH (KM)	LVC IN CRUST VEL. (KM/SEC)	LVC IN MANTLE DEPTH (KM)	LVC IN MANTLE VEL. (KM/SEC)
PENNSYLVANIA TO ARIZONA-NEW MEXICO AREA.						
OGD-ALQ,	63	26	NONE	-	100-120	4.37
SCP-ALQ,	73	40-50	NONE	-	120-140	4.46
SCP-TUC,	76	32	NONE	-	100+	4.52
TUC-BLA,	43	40	NONE	-	180+	4.22
TDNM-SCP,	50	40	NONE	-	80+	4.14
SKTX-BLWV,	38	38	NONE	-	160+	4.61
GEO-TUC,	74	32	NONE	-	100-120	4.34
SKTX-DHNY,	30	38	21-26	3.51	60+	4.76
SKTX-OGD,	36	32	21-26	3.40	60-80	4.59
FLO-TUC,	62	40	NONE	-	100+	4.12
FLO-ALQ,	64	38	21-26	3.51	100+	4.12
SOUTH-CENTRAL U.S. AREA.						
ATL-DRCO,	80	32-38	NONE	-	80-180	4.13
ATL-GOL,	83	32-38	21-26	3.54	80-180	4.20
GOL-ATL,	58	32	21-26	3.52	60+	4.22
ATL-DUG,	88	26	21-26	3.43	60+	4.10
OXF-RTNM,	84	38	21-26	3.53	60+	4.02
SHA-ALQ,	86	38	21-26	3.54	60-120	4.13
TUC-OXF,	29	38	NONE	-	140+	4.58
TUC-EUAL,	31	40	NONE	-	SEE TEXT.	
TUC-SHA,	33	38	21-26	3.56	100+	4.39
TUC-DAL,	35	38	NONE	-	60-160	4.21
SHA-LUB,	91	38	21-26	3.50	60+	4.04
LUB-ATL,	42	38	21-26	3.49	60+	4.00
LUB-OXF,	54	38	21-26	3.55	60-160	4.29
ATL-OXF,	79	38	NONE	-	100+	4.51

2. "Decoupling and Source Function for Explosions in a Three-Dimensional Model," by Dhari Saaid Bahjat, Digest of Ph.D. dissertation, May, 1968.

A three-dimensional model made of Plaster of Paris has been used to investigate some conditions of an explosion which control the seismic signal generated by such a source. This study is based on the idea that the seismic signal generated by an explosion can be reduced by detonating the explosive in a cavity. Spherical charges of chemical explosive are used to generate the seismic signal. The seismic waves are recorded at the surface of the model by calibrated capacitor receivers. The compressional wave velocity and absorption in Plaster of Paris are determined.

The factors which affect the seismic signal generated by the tamped explosion of a particular explosive material are the yield of the explosion, the depth of the explosion and the medium in which the explosion is buried. Data are collected for nine charge masses in the range from 20 to 162 milligrams. The results show that the peak amplitude of the compressional wave depends on 0.72 power of the yield. Also it is observed that the pulse width varies with the size of the charge. The dependence is 0.6 power of the yield.

Two series of experiments, one using 55 milligrams charges, the other 100 milligrams charges, have been conducted to investigate the variation of the peak amplitude of compressional waves with the cavity radius. The cavity radii are varied from 0.31 to 3.2 centimeters.

The amplitude of the compressional wave for a tamped shot is smaller than the one for cavity shots for the range of cavity sizes investigated. In the case of tamped shots, most of the energy released by the explosion is consumed in crushing the surrounding medium, and as waste heat deposited in the source region. The amplitude of the compressional wave increases as the cavity radius increases as long as the pressure applied to the surface of the cavity exceeds the compressive strength of the medium. The maximum amplitude is obtained for a cavity radius such that the stress transmitted through the wall of the cavity to the medium is equal to the compressive strength of the medium. The radius of the cavity in which the pressure applied on the surface of the cavity is equal to the compressive strength of the medium is a function of the charge mass. The amplitude decreases after reaching a maximum because of the reduction in the effective source region radius. Therefore, the factor by which the amplitude is reduced for a given increase in cavity radius is independent of the yield of the explosion.

The energy calculations verify that only a small fraction of the released energy is radiated into seismic waves. The seismic energy radiated in the P-wave is computed from the early part of the seismograms. It follows the same general pattern for increase and then decrease with increasing radius that the peak amplitude does. The radiated seismic energy for a tamped shot is shown to be less than for the cavity shots for this range of cavity sizes.

The idea that for some cavities the radius of the source region is larger than the radius of the given cavity is checked by observing the change in the pulse width of the first arrival. A minimum pulse width occurs at larger cavity radii for bigger charges. This is explained very well by the linear theory of a cavity in an infinite medium.

The maximum stress on the surface of the equivalent cavity is determined in two independent ways. First, starting from the point of explosion and proceeding outward from the source region to the elastic region, and secondly, starting from seismic waves observed at the surface of the model and moving inward to the elastic boundary around the source. The values of the peak stress obtained from equalization of recorded seismic waves to the surface of the cavity are in satisfactory agreement with the computed input stress to the medium for cavities which respond elastically. For overdriven cavities the input stress cannot be compared with that of calculated one from the seismic zone unless the decay of the stress in the fracture region is known.

3. "Exact Solution for the Displacement Components in $P_1P_2P_1$, $(S_1S_2S_1)_{SV}$, $(S_1S_2S_1)_{SH}$ Head Waves Due to an Impulsive Double Couple Source," by Umesh Chandra, in press, Bull. Seism. Soc. Am., 59 (1969)

Abstract

Exact integral expressions for the displacement components as a function of azimuth, in $P_1P_2P_1$, $(S_1S_2S_1)_{SV}$, and $(S_1S_2S_1)_{SH}$ head waves due to an impulsive double couple source of arbitrary orientation in two semi-infinite media separated by a plane horizontal boundary, and the effect of free surface on it, have been obtained. The time variation of the source is assumed to be represented by the Heaviside unit function. The response due to an arbitrary source excitation may, however, be obtained from this solution by superposition. Necessary formulae for the operational interpretation of integral equations occurring in the problem are given.

Illustrative examples showing the waveform in $P_1P_2P_1$, $(S_1S_2S_1)_{SV}$, and $(S_1S_2S_1)_{SH}$ head wave displacement components for a particular fault and a suitably chosen earth model are given. Plots of the projection of particle trajectory for P waves in u_r-u_z plane, and for S waves in u_φ-u_r and u_φ-u_z planes are given for different azimuths; where u_r, u_φ, u_z are the components of displacement in a cylindrical coordinate system (r, φ, z).

Unclassified
Security Classification

DOCUMENT CONTROL DATA - R&D

(Security classification of title, body of abstract and indexing annotation must be entered when the overall report is classified)

1. ORIGINATING ACTIVITY *(Corporate author)*
St. Louis University
St. Louis, Missouri 63103

2a. REPORT SECURITY CLASSIFICATION
Unclassified

2b. GROUP

3. REPORT TITLE
ANNUAL TECHNICAL REPORT

4. DESCRIPTIVE NOTES *(Type of report and inclusive dates)*
Scientific. Interim.

5. AUTHOR(S) *(First name, middle initial, last name)*
Carl Kisslinger
Otto W. Nuttli
William V. Stauder, S.J.
Seweryn J. Duda

6. REPORT DATE
1 September 1968

7a. TOTAL NO. OF PAGES
84

7b. NO. OF REFS
15

8a. CONTRACT OR GRANT NO. ARPA Order No. 292
AF19(628)-5100

b. PROJECT, TASK, WORK UNIT NOS.
8652-00-01

c. DOD ELEMENT 6250601R

d. DOD SUBELEMENT n/a

9a. ORIGINATOR'S REPORT NUMBER(S)

9b. OTHER REPORT NO(S) *(Any other numbers that may be assigned this report)*

10. DISTRIBUTION STATEMENT
1 - Distribution of this document is unlimited. It may be released to the Clearinghouse, Department of Commerce, for sale to the general public.

11. SUPPLEMENTARY NOTES
TECH, OTHER

12. SPONSORING MILITARY ACTIVITY
Air Force Cambridge Research Laboratories (CRJ)
L. G. Hanscom Field
Bedford, Massachusetts 01730

13. ABSTRACT

Research in seismology on fundamental problems related to the detection, location and identification of underground explosions is described. Work in progress pertains to studies of (1) long period P-wave amplitude anomalies at the Montana LASA, (2) determination of anomalous structure (in Fennoscandia) by use of first derivatives of P-wave travel times, (3) crust and mantle S-wave velocity distribution and its regional variations, (4) a new method of earthquake energy determination, (5) the effect of focal depth on the spectrum of body waves, and (6) the frequency dependence of transmission through a layer over a half-space examined by modeling seismology techniques. Completed research is summarized and has investigated (1) Love and Rayleigh wave phase velocities over U. S. continental paths, (2) decoupling and source function for explosions in a three-dimensional model, and (3) exact solutions for the displacement components in $P_1P_2P_1$, $(S_1S_2S_1)_{SV}$, $(S_1S_2S_1)_{SH}$ head waves due to an impulsive double couple source.

DD FORM 1 NOV 65 1473

Unclassified

14. KEY WORDS	LINK A		LINK B		LINK C	
	ROLE	WT	ROLE	WT	ROLE	WT
P-waves						
Large Aperture Seismic Array						
Travel Time Anomalies						
S-waves						
Earthquake Energy						
Seismic Modeling						
Surface Waves						
Head Waves						